Accuracy measurements of Bose-Einstein Condensates

Nøjagtigtheds målinger af Bose-Einstein kondensater

Author

Jeppe Juhl Thuesen

Student number: 201404267

Supervisor

Jan Arlt

University of Aarhus

Faculty of science

Department of physics and astronomy

June 14, 2019

Abstract

In the year 1995, Bose-Einstein Condensates were for the first time directly observed. This observation have since spurned other laboratories and today, countless Bose-Einstein condensates have been made and many interesting ideas have since been investigated in Bose-Einstein Condensates.

However there still seems to be discrepancies between theory and experimental realisations and the aim of this thesis is to be able to explain and correct for some of these discrepancies. The work of this thesis was mainly done in the Lattice Laboratory, which is a part of the Ultracold Quantum Gases Group at Aarhus University. The experiments happening in this laboratory are extra useful in this regard, due to the greater precision in measurements that is possible, due to the atom stabilisation we are utilising.

In this thesis I have worked on three different schemes in order to improve the ability to measure accurately. First, I have constructed a program to evaluate our atomic clouds, with a greater accuracy than before. Second, I worked together with the group in our investigation of the α-calibration, which previously have been done, but only took into account the effects from not being in an ideal two-level case and impure polarisation of the laser beam. With our investigation we have improved on this idea to include effects both from Doppler detuning and atomic densities, bringing us closer to a theory consistent with our measurements. Third, we investigated the possibility of another calibration parameter, this time we wish to make a correction to the scattering rate, which arises from collisions. This work was unfortunately not completed, as it proved harder to realise in our trap, than first anticipated.

Acknowledgements

The work in this thesis would have been a lot less comprehensive, if it had not been for the great and talented people I have had the pleasure and fortune to work with doing the work of my Master Thesis. I would like to first thank Mick and Mikkel, who have been excellent laboratory partners. I do not recall a day where we could not make stupid jokes, while taking our experimental data. And thank you for teaching me how the experiment works, with great patience, when I was a bit slow to understand what this button and that switch did. A huge thanks also for taking the time to proofreading parts of my thesis. Also a thanks to Toke, who joined the work in the laboratory half a year ago and bringing with him a sharp mind, able to ask the right questions, while bringing his excellent humour, making an already excellent atmosphere to work in, even better.

A big thanks to Jan Arlt also, for being a great supervisor, who made me feel welcome as a part of the group from the start and who always knew the last bit of the puzzle to make it all make sense.

Also a thanks to Thomas, Magnus and Nils from the Mixture laboratory, for valuable input to SkyFit and helping me understand what is going on in the Mixture laboratory.

Also a general thank you to the whole Ultracold Quantum gases group, for discussing constructive ideas, but also for having this sometimes very weird, but quite enjoyable talks over lunch or coffee.

Also a great thank you to Kasper Thrane for proofreading this thesis.

Contents

Chapter 1

Introduction

The beginning of the 20th century is marked by many great scientific milestones that broadened our understanding of the universe and everything considerably. One of the most important of these milestones is Quantum Mechanics both in terms of theoretical knowledge, but also in the form of technology, where many of our core technologies today, like the laser and transistor, would not be possible without Quantum Mechanics [1].

One part of Quantum Mechanics is the theory of Bose-Einstein Condensates, which began in the year 1924, when S.N. Bose wrote an article called *Planck's Law and the Hypothesis of Light Quanta* [2] and a letter to Einstein, asking him to translate it to German. Einstein agreed and was then inspired expand on this work, making the article named *Quantum theory of the monoatomic ideal gas* [3], which was the first article to ever touch the subject of Bose-Einstein condensation [4].

The work stood still for some years, until it was observed that ^{4}He showed new characteristics below ~ 2.17K, where a sudden absence of boiling, infinite thermal conductivity, zero viscosity in small channels, etc, was observed. [4]. In 1938, F. London coupled the superfluidity of ^{4}He together with the paper written by Einstein and hypothesised that the superfluidity of helium was due to a possible manifestation of BECs [5].

However direct evidence of Bose-Einstein condensation was not yet found. For many years further research was conduted, many great insights into ultracold quantum gases was acheived, like the contribution from N.N. Bogoliubov which really changed the understanding of interactions in Bose-Einstein Condensates [4]. However, it wasn't until 1995 where three groups independently found evidence of BECs in dilute atomic gases [6–8]. The reason for this long time from the first theoretical steps to the first experimental observation, is due to the required low temperatures, which

required laser-based techniques, such as laser cooling and magneto-optical trapping, which was first developed in the 1980s [5].

With an experimental observation, it became possible to actually see an almost macroscopic wave function, through optical methods [5]. As Bose-Einstein condensation is a quantum mechanical phenomenon it could also be used in a wide range of applications in the so called *second quantum revolution* [1].

As is generally the case for scientific studies, accuracy and precision are important, and this is no exception with Bose-Einstein condensates. As it will be shown in Chapter 2, there are a few approximations and assumptions made, that still separates theory from reality. Therefore the work in this thesis will focus on improving the accuracy of the measurements of Bose-Einstein Condensates in the Lattice laboratory at Aarhus University, by using methods that might be beneficial for the whole field. By trying to find a way to go from the theoretically approximated picture via calibrations, in order to achieve a higher resemblance with reality.

1.1 Thesis outline

The work in this thesis is focused on developing tools to improve our accuracy when doing evaluations of Bose-Einstein condensate absorption images. This work includes a few different investigations, which are somewhat independent of each other and therefore presented in different chapters. But they each is build on the same theoretical framework, therefore a dedicated chapter to theory have been written.

- **In Chapter 1** is the introduction you are reading right now.
- **In Chapter 2** is a chapter dedicated to theory, with a few assumption based on our specific experimental set-up, where Bose-Einstein condensates are explained together with the interaction between atoms and light in a two-level system.
- **In chapter 3** there is an overview of the experimental sequence done in order to produce Bose-Einstein condensates, together with all the small experiments done in order to optimise said sequence.
- **In chapter 4** describes the Matlab program I wrote in order to improve the groups standard evaluation of the images taken of the atoms.
- **In chapter 5** outlines the work we did in order to improve the α-calibration already done in the laboratory.

- **In chapter 6** describes the work in regard to finding the β-parameter, in order to make corrections to the scattering rate.

- **In chapter 7** shows my conclusions and outlook of the work of the above three chapters.

Chapter 2

Understanding BEC measurements

2.1 Bose-Einstein condensates

The atomic clouds produced in the laboratory can be in two different phases, they can either be in a thermal cloud, which is a gas cloud following semi-classic thermodynamic laws. The other phase is a phase that happens when classic thermodynamics breaks down and quantum mechanics takes over, and the cloud becomes an atomic quantum gas. Depending on whether the is cloud made of bosons or fermions, the cloud can then be described by either Bose-Einstein statistics or Fermi-Dirac statistics. In this thesis work, only the bosonic case is relevant. This means for non-interacting indistinguishable particles, the occupancy of the state i with energy ϵ_i can be described by the distribution function,

$$f_i^0(\epsilon_i) = \frac{1}{e^{(\epsilon_i - \mu)/k_b T} - 1}, \tag{2.1}$$

where μ is the chemical potential, k_b is Boltzmann's constant and T is the temperature. While being confined in a 3D harmonic potential, which can be described as (for more detail see Section 3.2),

$$U(x, y, z) = \frac{1}{2} m(\omega_x^2 x^2 + \omega_y^2 y^2 + \omega_z^2 z^2), \tag{2.2}$$

where ω_j is what is called the trap frequency in the j'th direction.

All states in Eq. (2.13) where $i > 0$ are excited states and we denote the atoms in these states, as thermal atoms. To find the amount of thermal atoms, we can sum up all states with $i > 0$, this can then be an integral by introducing the density of

states, $g(\epsilon)$ [9],

$$N_{th} = \sum_{i \neq 0} \frac{1}{e^{(\epsilon_i - \mu)/k_b T} - 1} \Rightarrow \int_0^\infty \mathrm{d}\epsilon \frac{g(\epsilon)}{e^{(\epsilon_i - \mu)/k_b T} - 1}, \tag{2.3}$$

where the density of states is given as,

$$g(\epsilon) = \frac{\epsilon^2}{2\hbar^3 \omega_x \omega_y \omega_z}. \tag{2.4}$$

Eq. (2.3) can be solved and gives,

$$N_{th} = \frac{\zeta(3)(k_b T)^3}{\hbar^3 \omega_x \omega_y \omega_z}, \tag{2.5}$$

where $\zeta(x)$ is the Riemann zeta function. The phase change to the quantum mechanical regime, happens when the temperature of the atomic cloud approach the absolute zero temperature, this stems from Louis de Broglie's postulate of the wave like behaviour of matter, where the wavelength can be described as,

$$\lambda_{dB} = \frac{h}{p} = \sqrt{\frac{2\pi\hbar^2}{m k_b T}}, \tag{2.6}$$

where p and, m is the momentum and mass of the atom, respectively. This number is small for thermal atoms, but when T becomes even smaller, the wavelength gets larger and at some point close to absolute zero, the wavelength becomes comparable to the average distance between the atoms. For the bosonic case, this will mean the waves of the atoms will begin to overlap and this is where a Bose-Einstein condensate is formed. When this happens all of the atoms share the same quantum state and coherently the same macroscopic wave function, due to their bosonic nature [10]. One way to set up the requirement for a cloud to be a BEC is as[10],

$$\rho_{PS}(T) = n\lambda_{dB}^3(T) = n\left(\frac{2\pi\hbar^2}{m k_b T}\right)^{3/2} \approx 2.612 \tag{2.7}$$

where ρ_{PS} is what is called phase space density and n is the density. With this definition we can find the temperature where the phase change happens,

$$T_c \approx \left(\frac{n}{2.612}\right)^{2/3} \frac{2\pi\hbar^2}{m k_b}. \tag{2.8}$$

We can also denote the critical temperature, as the temperature where all atoms are in excited states,

$$N = N_{th} = \frac{\zeta(3)(k_b T_c)^3}{\hbar^3 \omega_x \omega_y \omega_z} \Rightarrow k_b T_c = \frac{\hbar(\omega_x \omega_y \omega_z)^{1/3}}{\zeta(3)^{1/3}} N^{1/3}. \tag{2.9}$$

The amount of BEC atoms at all temperatures is then $N_{BEC} = N - N_{th}$. Which means we can describe the fraction of BECs as;

$$\frac{N_{BEC}}{N} = \frac{N - N_{th}}{N} = 1 - \left(\frac{T}{T_c}\right)^3. \tag{2.10}$$

This the condensate fraction for an ideal non-interacting gas.

If we wish to find the density distribution of the thermal atoms, we can use the semi-classical approximation, where the discrete energies are replaced by continuous energy of a particle in an external potential,

$$\epsilon_i \rightarrow \epsilon_{\mathbf{p}}(\mathbf{r}) = \frac{p^2}{2m} + U(\mathbf{r}), \tag{2.11}$$

where U is the external potential. This approximation is valid when the thermal energy is much larger than the level spacing of the potential [11]. To get the spatial density distribution the distribution function $f^0(\mathbf{r}, \mathbf{p})$ is integrated over momentum, as $f^0(\mathbf{r}, \mathbf{p})\mathrm{d}\mathbf{r}\mathrm{d}\mathbf{p}$ is the number of particles in a phase space volume element. This leads to a spatial density distribution,

$$n_{th}(\mathbf{r}) = \int \frac{\mathrm{d}\mathbf{p}}{(2\pi\hbar)^3} \frac{1}{e^{(p^2/2m + U(\mathbf{r}) - \mu)/k_b T} - 1}, \tag{2.12}$$

where the solution to this is,

$$n_{th}(\mathbf{r}) = \frac{1}{\lambda_{dB}^3} g_{3/2}\left(e^{(\mu - U(\mathbf{r}))/k_b T}\right), \tag{2.13}$$

where $g_{3/2}$ is the Bose function (also called the polylogarithm function)

$$g_j(\chi) = \sum_{i=1}^{\infty} \frac{\chi^i}{i^j}. \tag{2.14}$$

This means Eq. (2.13) can be rewritten as,

$$n_{th}(\mathbf{r}) = \frac{N}{(2\pi)^{3/2}\sigma_x\sigma_y\sigma_z g_3(\tilde{z})} g_{3/2}\left(\tilde{z} e^{-\sum_{i=x,y,z} r_i^2/2\sigma_i^2}\right), \tag{2.15}$$

where the fugacity, $\tilde{z} = e^{\mu/k_b T}$ and the cloud width, $\sigma_i = \sqrt{k_b T/m\omega_i^2}$.

In the limit of high temperature (i.e. $T \gg T_c$), then $\tilde{z} \ll 1$, which leads to only the first term in the Bose function (Eq. (2.14)) contributes and the density distribution becomes,

$$n_{th}^{\mathrm{MB}}(\mathbf{r}) = \frac{N}{(2\pi)^{3/2}\sigma_x\sigma_y\sigma_z} e^{\sum_i r_i^2/2\sigma_i^2}, \tag{2.16}$$

which is a classical Maxwell-Boltzmann distribution. Even if the thermal atoms are calculated in the non-interacting case, Eq. (2.15) is valid when the describing thermal atoms in trap.

2.1.1 Interacting BECs

To find the density distribution of the BEC atoms another route is needed. The approximation of non-interacting atoms, is no longer really viable, if we want an

answer close to reality. The many-body Hamiltonian describing N interacting bosons confined in an external potential U is in second quantisation given as [5],

$$\hat{H} = \int \mathrm{d}\mathbf{r}\hat{\Psi}^\dagger(\mathbf{r})\left[-\frac{\hbar^2}{2m}\nabla^2 + U\right]\hat{\Psi}(\mathbf{r}) + \frac{1}{2}\int \mathrm{d}\mathbf{r}\mathrm{d}\mathbf{r}'\hat{\Psi}^\dagger(\mathbf{r})\hat{\Psi}^\dagger(\mathbf{r}')U_s(\mathbf{r}-\mathbf{r}')\hat{\Psi}(\mathbf{r}')\hat{\Psi}(\mathbf{r}), \quad (2.17)$$

where $\hat{\Psi}^\dagger(\mathbf{r})$ and $\hat{\Psi}(\mathbf{r})$ are the annihilation and creation field operators for particles at position $\mathbf{r}$. The first integral describes a single particle moving in an external field, while the second describes the interaction between particles, though the two-body inter-atomic scattering potential $U_s(\mathbf{r}-\mathbf{r}')$. As this is used to describe BECs, we can safely assume they are ultracold, which means the collisions are completely dominated by s-wave scattering events, which is parametrised by the scattering length, a [5].

If the inter-atomic separation is large compared to this scattering length, then the potential can be viewed as a contact interaction, which means the inter-atomic scattering potential can be rewritten as [5],

$$U_s = U_0\delta(\mathbf{r}-\mathbf{r}'), \quad (2.18)$$

where $U_0 = 4\pi\hbar^2/m$. Then the field operator is split up into two terms [11],

$$\hat{\Psi}(\mathbf{r},t) = \Phi(\mathbf{r},t) + \hat{\Psi}'(\mathbf{r},t), \quad (2.19)$$

where $\Phi(\mathbf{r},t)$ is defined as the expectation value of the field operator $\Phi(\mathbf{r},t) \equiv \langle\hat{\Psi}(\mathbf{r},t)\rangle$, this leads to $n_0(\mathbf{r},t) = |\Phi(\mathbf{r},t)|^2$ and $\hat{\Psi}'(\mathbf{r},t)$ represents the fluctuations of the excitations. Using Heisenberg's equation it follows,

$$i\hbar\frac{\partial}{\partial t}\Phi(\mathbf{r},t) = \left[-\frac{\hbar^2\nabla^2}{2m} + U(\mathbf{r}) + U_0|\Phi(\mathbf{r},t)|^2\right]\Phi(\mathbf{r},t), \quad (2.20)$$

this is the famous time-dependat Gross-Pitaevskii equation, which we can further simplify by separating time from space, $\Phi(\mathbf{r},t) = \psi(\mathbf{r})\exp(-i\mu t/\hbar)$ leading to,

$$\mu\psi(\mathbf{r}) = \left[-\frac{\hbar^2\nabla^2}{2m} + U(\mathbf{r}) + U_0 n_0(\mathbf{r})\right]\psi(\mathbf{r}), \quad (2.21)$$

yielding the stationary Gross-Pitaevskii equation. This can be simplified further by utilising the Thomas-Fermi approximation, which states that for zero temperature the kinetic term can be neglected,

$$\mu\psi(\mathbf{r}) = [U(\mathbf{r}) + U_0 n_0(\mathbf{r})]\psi(\mathbf{r}). \quad (2.22)$$

This means it is possible to isolate the density distribution,

$$n_0(\mathbf{r}) = \frac{\mu - U(\mathbf{r})}{U_0}, \quad \mu - U(\mathbf{r}) > 0 \quad (2.23)$$

for the anisotropic three-dimensional harmonic trap potential seen in Eq. (2.2), the cloud can be described as,

$$n_0(x,y,z) = n(0)\left(1 - \frac{x^2}{R_x^2} - \frac{y^2}{R_y^2} - \frac{z^2}{R_z^2}\right), \quad \mu - U(\mathbf{r}) > 0, \tag{2.24}$$

where $x = y = z = 0$ is the center of the cloud and R_i is the Thomas-Fermi radii, given as,

$$R_i = \sqrt{\frac{2\mu}{m\omega_i}}. \tag{2.25}$$

Requiring normalisation of $\Phi(\mathbf{r},t)$ ($\int |\Phi(\mathbf{r},t)|^2 \mathrm{d}\mathbf{r} = N$), the chemical potential, μ, can easily be found,

$$\mu = \frac{1}{2}[(15N_0a)^2 m\hbar^4(\omega_x\omega_y\omega_z)^2]^{1/5}. \tag{2.26}$$

Which tells us, the atom number and the size of the BEC to be coupled together through the chemical potential.

Returning to the condensate fraction, these interactions will change (2.10). The number of thermal atoms are given as,

$$N_{th} = \int \frac{\mathrm{d}\mathbf{r}\mathrm{d}\mathbf{p}}{(2\pi\hbar)^3} \frac{1}{\exp[p^2/2m + U(\mathbf{r}) - \mu)/k_bT] - 1}. \tag{2.27}$$

Explicit integration, using the Thomas-Fermi approximation for the effective mean-field potential, $U - \mu = |U_{ext}(\mathbf{r}) - \mu|$ leads to [5],

$$\frac{N_{BEC}}{N} = 1 - \left(\frac{T}{T_c}\right)^3 - \frac{\zeta(2)}{\zeta(3)}\eta\left(\frac{T}{T_c}\right)^2\left(1 - \left(\frac{T}{T_c}\right)^3\right)^{2/5}, \tag{2.28}$$

where $\eta = \mu/k_bT_c$. This is still not an exact solution and is only valid to the lowest order of η and should only be used to get a qualitative understanding on the role of interaction [11].

2.1.2 Expansion

With a description of how the atoms behave in an harmonic trap, we take it one step further, which is to describe how the atoms behave in free fall. As is described in more detail in Chapter 3, the trap is at some point turned off and the atoms are then no longer confined in any trap and the behaviour of both the thermal and BEC atoms under these conditions become relevant.

Thermal cloud

We have the trapping potential defined in Eq. (2.2), this trap is turned off at $t = 0$, where t denotes the time the atoms have been in flight, often called time of flight

(ToF). If we neglect gravity and collisions, the position of each atom during time of flight can be described as,

$$\mathbf{r} = \mathbf{r}_0 + \frac{\mathbf{p}}{m}t, \tag{2.29}$$

where $\mathbf{r}_0$ is the initial position of the atom and $\mathbf{p}$ and m is the atoms momentum and mass. This means we can rewrite the distribution function, $f^0(\mathbf{r}, \mathbf{p})$, to,

$$f^0(\mathbf{r} - \frac{\mathbf{p}t}{m}, \mathbf{p}) = \frac{1}{e^{(p^2/2m + U(\mathbf{r}-\mathbf{p}t/m)-\mu)/k_bT} - 1}. \tag{2.30}$$

Then by modifying Eq. (2.12) with the new distribution function,

$$n_{th}(\mathbf{r}, t) = \int \frac{\mathrm{d}\mathbf{p}}{(2\pi\hbar)^3} \frac{1}{e^{(p^2/2m + U(\mathbf{r}-\mathbf{p}t/m)-\mu)/k_bT} - 1}. \tag{2.31}$$

In the case of a harmonic potential, we can solve this by a change of coordinates that separates spatial coordinates and momentum [11], leading to a solution of the form,

$$n_{th}(\mathbf{r}, t) = \frac{N}{(2\pi\hbar)^{3/2} w_x w_y w_z g_3(\tilde{z})} g_{3/2}\left(\tilde{z} e^{-\sum_i r_i^2/2w_i^2}\right), \tag{2.32}$$

where the width of the cloud at a given Time of Flight, t, is,

$$w_i(t) = \sqrt{\frac{k_bT}{m\omega_i^2}\left(\frac{1}{\omega_i^2} + t^2\right)} = \sigma_i \sqrt{\frac{1}{\omega_i^2} + t^2}. \tag{2.33}$$

Bose-Einstein condensates

To describe the quantum mechanical phenomenon of BEC expansion, some classical Newtonian observations can be made. For any time, be it in trap or in free expansion, the force each atom experiences can be written as [12],

$$\mathbf{F}(\mathbf{r}, t) = -\nabla(U(\mathbf{r}, t) + U_0 n_o(\mathbf{r}, t)), \tag{2.34}$$

where $t = 0$ is when the trap is turned off, which means $\mathbf{F}(\mathbf{r}, 0) = 0$, as we assume the cloud is in equilibrium. A rather straightforward parametrisation can also be made in regard to the radius of the BEC at any time,

$$R_i(t) = \lambda_i(t) R_i(0) \quad (i = x, y, z), \tag{2.35}$$

where $\lambda_i(t)$ is called the scaling parameter that starts out as $\lambda(0) = 1$. From this ansatz the evolution of the spatial density evolution can be found,

$$n_0(\mathbf{r}, t) = \frac{n_0(r_x/\lambda_x(t), r_y/\lambda_y(t), r_z/\lambda_z(t), 0)}{\lambda_x(t)\lambda_y(t)\lambda_z(t)} \tag{2.36}$$

By utilising Newton's 2nd law, $m\ddot{R}_i(t) = F_i[\mathbf{R}(t), t]$, on the trajectory and that using $\mathbf{F}(\mathbf{r}, 0) = 0, \Rightarrow \nabla U_0 n_0(t = 0) = -\nabla U(t = 0)$, we arrive at,

$$m\ddot{\lambda}_i(t) R_i(0) = -\partial_i U(\mathbf{R}(t), t) + \frac{\partial_i U(\mathbf{R}(0), 0)}{\lambda_i \lambda_x \lambda_y \lambda_z}. \tag{2.37}$$

Given the harmonic potential described in Eq. (2.2), both sides of the equation is proportional to $R_j(0)$, which is interesting, as this means the scaling is independent of the in-trap size of the BEC and thus validating Eq. (2.35) as long as $\lambda_i(t)$ satisfies,

$$\ddot{\lambda}_i = \frac{\omega_i^2(0)}{\lambda_i\lambda_1\lambda_2\lambda_3} - \omega_i(t)\lambda_i. \tag{2.38}$$

Doing the same tricks as for the in-trap BEC calculations previously, we then arrive at a spatial density distribution of [12],

$$n_0(\mathbf{r},t) = \frac{\mu - U(\mathbf{r},0)}{U_0\lambda_x(t)\lambda_y(t)\lambda_z(t)} = \frac{\mu - \sum_i \frac{1}{2}m\omega_i^2 r_i^2/\lambda_i(t)}{U_0\lambda_x(t)\lambda_y(t)\lambda_z(t)} \tag{2.39}$$

Leading again, to the reverse parabola,

$$n_0(x,y,z,t) = \frac{15N_0}{8\pi R_x(t)R_y(t)R_z(t)}\left(1 - \frac{x^2}{R_x^2(t)} - \frac{y^2}{R_y^2(t)} - \frac{z^2}{R_z^2(t)}\right) \quad \text{for} \quad \mu > U(\mathbf{r},0), \tag{2.40}$$

where the radius is now defined as,

$$R_i(t) = \sqrt{\frac{2\mu}{m\omega_j}}\lambda_i(t) = \left(\frac{15\hbar^2 a\bar{\omega}^3 N_{BEC}}{\omega_j}\right)^{2/5}\frac{\lambda_i(t)}{m^{2/5}}. \tag{2.41}$$

As will be further elaborated in Sec. 3.2, there are actually only two trap frequencies in the QUIC-trap utilised, which are the axial (ω_a) and radial (ω_r) trap frequencies. The aspect ratio between these two, can at any time be described as,

$$\frac{w_r(t)}{w_a(t)} = \frac{\lambda_r(t)\sqrt{2\mu/m\omega_r^2}}{\lambda_a(t)\sqrt{2\mu/m\omega_a^2}} = \epsilon\frac{\lambda_r(t)}{\lambda_a(t)} \tag{2.42}$$

where $\epsilon = \omega_a/\omega_r$, which in this case is $\epsilon \ll 1$, telling us that in-trap, the BEC takes the form of a cigar. What form these λ take, can be solved numerically by using Eq. (2.38). To get an idea of the expansion of the BEC, we can consider the simplest case, where the trap is instantaneously turned off at $t = 0$. If the trap is turned off instantaneously, the second term becomes zero as the atoms no longer feel any confinement from the trap for all $t > 0$, this leads to Eq. (2.38) can be simplified to,

$$\begin{aligned}\frac{\mathrm{d}^2\lambda_r}{\mathrm{d}\tau^2} &= \frac{1}{\lambda_r^3\lambda_z},\\ \frac{\mathrm{d}^2\lambda_a}{\mathrm{d}\tau^2} &= \frac{\epsilon^2}{\lambda_r^2\lambda_z^2},\end{aligned} \tag{2.43}$$

where τ is a dimensionless time variable $\tau = \omega_r(0)t$. This can be solved by doing an expansion in powers of ϵ [12]. To zeroth order in ϵ, $\lambda_a = 1$ and the radial scaling parameter becomes,

$$\lambda_r(\tau) = \sqrt{1+\tau^2}. \tag{2.44}$$

To second order in ϵ, the axial scaling parameter becomes,

$$\lambda_a(\tau) = 1 + \epsilon(\tau \arctan \tau - \ln \sqrt{1+\tau}). \tag{2.45}$$

Given that $\epsilon \ll 1$ it is easily seen that the radial expansion grows much faster than the axial expansion, leading our cigar shaped cloud to become a pancake at high time of flight, with its two major axes being the those that initially was the minor axes. This is quite remarkable, as it means the atoms accelerate much faster in two of the three directions than the last, even though there are no external forces acting upon them.

2.2 Atom-light Interactions

In the experiment we use atoms and light in order to gain information about the atoms and their properties, therefore it might be useful to explore the theory behind this interaction. To achieve this the Optical Bloch equations can be utilised, as these can describe a two-level atom interacting with an electromagnetic field. In the experiment we are working with ^{87}Rb and we assume we have a pure polarisation of the light, to a good approximation, we can treat it like a two-level system.

A wavefunction of a pure two-level atom can be written as,

$$\Psi(\mathbf{r}, t) = c_g(t) \left|g\right\rangle + c_e(t) \left|e\right\rangle e^{-i\omega_0 t}, \tag{2.46}$$

where $|c_i|^2$ is the probability to be in the i'th state and ω_0 is the resonance frequency between the two states. The evolution of the system can be described by the time-dependant Schrödinger equation,

$$i\hbar \frac{\mathrm{d}\Psi(\mathbf{r}, t)}{\mathrm{d}t} = H\Psi(\mathbf{r}, t). \tag{2.47}$$

The Hamiltonian can be split into two parts, $H = H_0 + H_I(t)$, where H_0 describes the energy of the unperturbed system and $H_I(t)$ describes the interaction with the oscillating electric field. Then we assume that it is only the interaction between the electric part of the radiation and the electric dipole moment with a single electron that drives the transition, known as the electric dipole approximation [13]. Under the further assumption that the radiation can be treated as a plane wave, the interaction Hamiltonian can be written as,

$$H_I(t) = \mathbf{d} \cdot \mathbf{E}(t) = e\mathbf{r} \cdot \mathbf{E}_0 \cos(\omega_L t), \tag{2.48}$$

where $\mathbf{d}$ is the electric dipole moment of the atom, $\mathbf{E}$ is the electric field and ω_L is the frequency of the laser radiation, used to drive the transition. Then by using Eqs.

(2.46) and (2.47),

$$i\hbar\frac{\mathrm{d}c_g(t)}{\mathrm{d}t} = c_e \langle g| \mathbf{d}\cdot\mathbf{E} |e\rangle e^{-i\omega_0 t} = c_e\Omega^*\hbar\left(\frac{e^{i(\omega_L-\omega_0)t}+e^{-i(\omega_L+\omega_0)t}}{2}\right) \tag{2.49}$$

$$i\hbar\frac{\mathrm{d}c_e(t)}{\mathrm{d}t} = c_g \langle e| \mathbf{d}\cdot\mathbf{E} |g\rangle e^{+i\omega_0 t} = c_g\Omega\hbar\left(\frac{e^{i(\omega_L+\omega_0)t}+e^{-i(\omega_L-\omega_0)t}}{2}\right), \tag{2.50}$$

where one of the key parameters for atom-light interaction appears, the Rabi frequency, Ω, which is given as,

$$\Omega = \frac{\langle e| \mathbf{d}\cdot\mathbf{E} |g\rangle}{\hbar} = \frac{eE_0}{\hbar}\langle e| \mathbf{r}\cdot\hat{\mathbf{E}} |g\rangle . \tag{2.51}$$

Another approximation that can be made is the Rotating Wave Approximation (RWA), where we assume terms of $e^{i(\omega_L+\omega_0)t}$ oscillates much faster than terms of $e^{i(\omega_L-\omega_0)t}$. Because the plus terms oscillate that much faster we can see them as being averaged out over a period of the minus terms. This is a very good approximation in the case where the frequency of the radiation is close to the atomic frequency and we are in the optical regime where the frequency is on the order of 10^{14}Hz. This leads to Eqs. (2.49) and (2.50) can be simplified as [20],

$$i\dot{c_g}(t) = c_e\Omega^*\frac{e^{i\Delta t}}{2} \quad \text{and} \quad i\dot{c_e}(t) = c_g\Omega^*\frac{e^{-i\Delta t}}{2}, \tag{2.52}$$

where $\Delta = \omega_L - \omega_0$, which is called the detuning.

By using the density operator, $\rho = |\Psi\rangle\langle\Psi|$ on the wavefunction, the density matrix is made,

$$\rho = \begin{pmatrix} c_e c_e^* & c_e c_g^* \\ c_g c_e^* & c_g c_g^* \end{pmatrix}. \tag{2.53}$$

the time evolution of the density matrix can then be found, as an example the time evolution of ρ_{gg} is then,

$$\frac{\mathrm{d}\rho_{gg}}{\mathrm{d}t} = \frac{\mathrm{d}c_g}{\mathrm{d}t}c_g^* + c_g\frac{\mathrm{d}c_g^*}{\mathrm{d}t} = -i\frac{\Omega^*}{2}\tilde{\rho}_{eg} + i\frac{\Omega}{2}\tilde{\rho}_{ge}, \tag{2.54}$$

where $\tilde{\rho}_{ge} = \rho_{ge}e^{i\Delta t}$. In order to describe a real atomic system one key parameter is still missing, and that is the spontaneous decay of the excited state, which we can write as [20],

$$\left.\frac{\mathrm{d}\rho_{ee}}{\mathrm{d}t}\right|_{spon} = -\left.\frac{\mathrm{d}\rho_{gg}}{\mathrm{d}t}\right|_{spon} = -\Gamma\rho_{ee}, \tag{2.55}$$

where Γ is the lifetime of the excited state. This motivates a complete set of equations

of the density matrix,

$$\begin{aligned}
\frac{\mathrm{d}\rho_{gg}}{\mathrm{d}t} &= \Gamma\rho_{ee} + \frac{i}{2}(\Omega\tilde{\rho}_{ge} - \Omega^*\tilde{\rho}_{eg}) \\
\frac{\mathrm{d}\rho_{ee}}{\mathrm{d}t} &= -\Gamma\rho_{ee} + \frac{i}{2}(\Omega\tilde{\rho}_{eg} - \Omega^*\tilde{\rho}_{ge}) \\
\frac{\mathrm{d}\tilde{\rho}_{ge}}{\mathrm{d}t} &= -\left(\frac{\Gamma}{2} + i\Delta\right)\tilde{\rho}_{ge} + \frac{i}{2}(\Omega^*(\rho_{gg} - \rho_{ee}) \\
\frac{\mathrm{d}\tilde{\rho}_{eg}}{\mathrm{d}t} &= -\left(\frac{\Gamma}{2} - i\Delta\right)\tilde{\rho}_{eg} + \frac{i}{2}(\Omega(\rho_{ee} - \rho_{gg}).
\end{aligned} \tag{2.56}$$

These set of equations are what is called the Optical Bloch Equations [13]. To describe a closed two-level system it is required that for all times $\rho_{gg} + \rho_{ee} = 1$, which also means $\dot{\rho}_{gg} = -\dot{\rho}_{ee}$ and thus reducing the amount of free variables by one. Then we can introduce the population difference, w,

$$w = \rho_{ee} - \rho_{gg}. \tag{2.57}$$

To obtain an expression for the absorption of light, we find the steady state solution to Eq. 2.56, this is simplified by using, $\rho_{eg} = \rho_{ge}^*$, which gives us two equations,

$$\frac{\mathrm{d}\tilde{\rho}_{eg}}{\mathrm{d}t} = -\left(\frac{\Gamma}{2} - i\Delta\right)\tilde{\rho_{eg}} + \frac{i\Omega}{2}w \tag{2.58}$$

and

$$\frac{\mathrm{d}w}{\mathrm{d}t} = -\Gamma w + i(\Omega^*\tilde{\rho}_{eg} - \Omega\rho_{eg}^*) - \Gamma. \tag{2.59}$$

By requiring steady state, makes $\frac{\mathrm{d}\tilde{\rho}_{eg}}{\mathrm{d}t} = \frac{\mathrm{d}w}{\mathrm{d}t} = 0$, using this in Eq. (2.58) and isolating $\tilde{\rho}_{eg}$ gives,

$$\tilde{\rho}_{eg} = \frac{i\Omega}{2(\Gamma/2 - i\Delta)}w. \tag{2.60}$$

To determine the steady-state w we first solve, $(\Omega^*\tilde{\rho} - \Omega\tilde{\rho})/w$,

$$\begin{aligned}
\frac{\Omega^*\tilde{\rho} - \Omega\tilde{\rho}^*}{w} &= \frac{i\Omega^*\Omega}{2(\Gamma/2 - i\Delta)} + \frac{i\Omega^*\Omega}{2(\Gamma/2 + i\Delta)} \\
&= \frac{i|\Omega|^2}{2}\frac{(\Gamma/2 + i\Delta) + (\Gamma/2 - i\Delta)}{(\Gamma/2 + i\Delta)(\Gamma/2 - i\Delta)} \\
&= \frac{i|\Omega|^2}{2}\frac{\Gamma}{(\Gamma/2)^2 + \Delta^2} \\
&= i\frac{2|\Omega|^2}{\Gamma^2}\frac{\Gamma}{1 + \left(\frac{2\Delta}{\Gamma}\right)^2} \\
&= is_0\frac{\Gamma}{1 + \left(\frac{2\Delta}{\Gamma}\right)^2} = i\Gamma s(\Delta).
\end{aligned}$$

Here we have introduced the saturation parameter, which is given as,

$$s(\Delta) = \frac{s_0}{1 + \left(\frac{2\Delta}{\Gamma}\right)^2}, \tag{2.61}$$

where the on resonance saturation parameter is $s_0 = 2|\Omega|^2/\Gamma^2$. Using this in Eq. (2.59) with the steady-state condition, yields a new expression for the population difference,

$$w = \frac{-1}{1 + s(\Delta)}. \tag{2.62}$$

The intensity of the light interacting with the atom can be written as,

$$I = \frac{\epsilon_0 c E_0^2}{2}. \tag{2.63}$$

Because both the intensity and the Rabi frequency, $|\Omega|^2$ (Eq. (2.51)) can be described with the strength of the electric field of the light, the Rabi frequency can be rewritten in terms of the intensity,

$$|\Omega|^2 = \frac{2I}{\epsilon_0 c\hbar^2}(\langle e|\,\mathbf{r}\cdot\hat{\mathbf{E}}\,|g\rangle)^2, \tag{2.64}$$

which means the on-resonance saturation parameter also can be written as,

$$s_0 = \frac{4I}{\epsilon_0 c\hbar^2\Gamma^2}(\langle e|\,\mathbf{r}\cdot\hat{\mathbf{E}}\,|g\rangle)^2 = \frac{I}{I_s}, \tag{2.65}$$

where I_s is what we call the saturation intensity and is given as,

$$I_s = \frac{\epsilon_0 c\hbar^2\Gamma^2}{4(\langle e|\,\mathbf{r}\cdot\hat{\mathbf{E}}\,|g\rangle)^2}. \tag{2.66}$$

In the experiment we use circularly polarised light, this means we can write it as [14],

$$I_{s,\text{circ}} = \frac{\hbar\omega_0^3\Gamma}{12\pi c^2}, \tag{2.67}$$

for the rest of this thesis we will assume $I_s = I_{s,\text{circ}}$.

In steady state the excitation rate and the decay rate are equal and since the population in the excited state decays at a rate Γ, the total photon scattering rate R can be given as [20],

$$R = \Gamma\rho_{ee} = \frac{\Gamma}{2}\frac{s_0}{1 + s - 0 + \left(\frac{2\Delta}{\Gamma}\right)^2} = \frac{\Gamma}{2}\frac{I/I_s}{1 + I/I_s + \left(\frac{2\Delta}{\Gamma}\right)^2}. \tag{2.68}$$

The amount of scattered power per unit of volume is given as $\hbar\omega_L nR$, which means we can describe the attenuation of the laser as,

$$\frac{\mathrm{d}I'}{\mathrm{d}z} = -\hbar\omega_L Rn = -\sigma n I', \tag{2.69}$$

where σ is the the cross-section and is given as,

$$\sigma = \frac{\hbar\omega_L\Gamma}{2I_s}\frac{1}{1 + I/I_s + \left(\frac{2\Delta}{\Gamma}\right)^2} = \frac{\sigma_0}{1 + I/I_s + \left(\frac{2\Delta}{\Gamma}\right)^2}, \tag{2.70}$$

where,

$$\sigma_0 = \frac{\hbar\omega_L\Gamma}{2I_s}, \tag{2.71}$$

which is the on-resonance cross section.

2.3 Absorption imaging

In order to do any real science, measurements are essential. So in order to use the results of Section 2.1, we will have to find a way to see the spatial distributions described here. This can be done through absorption imaging. The first thing to consider, is that an atomic cloud is of course a three-dimensional object, but as it often happens, such things can be put down to 2D, this is done through what we call column density,

$$\tilde{n}(x,y) = \int n(x,y,z)\mathrm{d}z, \tag{2.72}$$

Then the differential equation, Eq. (2.69), can be solved, yielding,

$$\mathrm{OD} = \sigma_0 \int_0^\infty n\,\mathrm{d}z = \sigma_0 \tilde{n} = \left(1 + \left(\frac{2\Delta}{\Gamma}\right)^2\right) \ln\left(\frac{I_0}{I}\right) + \frac{I_0 - I}{I_s} \tag{2.73}$$

where OD is the optical depth, I and I_0 are the intensities of the laser in the image with and without atoms, respectively. As both I and I_0 are measurable quantities and with the relation between the optical depth and the column density, it is then straightforward to get information about the atomic cloud.

2.3.1 Imaging corrections

Eq. (2.73) is an expression of the ideal case, as this thesis is built on experimental work, some corrections have to be made in order to get Eq. (2.73) to match with the actual experimental results. The first wrong assumption in Eq. (2.73) is that the only light in the image is the laser light. Another assumption is in regard to the saturation intensity, I_s, as this is a quantity for the ideal two-level case, which is not really the case in reality. In the scattering rate, Γ, there is also the assumption of no collisions, which again, is not entirely true.

The first correction, corrects the assumption that the only light in the image is the laser light. The laser light is by far the strongest source of intensity, but there might still be some light pollution from other sources. This could make the OD of the cloud higher than it actually is. This can easily be remedied by taking another image, this time without both laser light and atoms. This is done twice, with the same time separation as the atom and beam image, this way eventual camera effects will be accounted for. This leads to

$$I = I_{\mathrm{atom}} - I_{\mathrm{atom,bias}} \quad \text{and} \quad I_0 = I_{\mathrm{beam}} - I_{\mathrm{beam,bias}}. \tag{2.74}$$

To summarise, when doing an experimental procedure there is first taken an image with a laser beam and an atomic cloud (I_{atom}), then when the atoms are gone,

another image is taken (I_{beam}) and then lastly the laser is turned off and the two bias images are taken ($I_{\text{atom,bias}}$ and $I_{\text{atom,bias}}$). An example of these three can be seen on Figure 2.1.

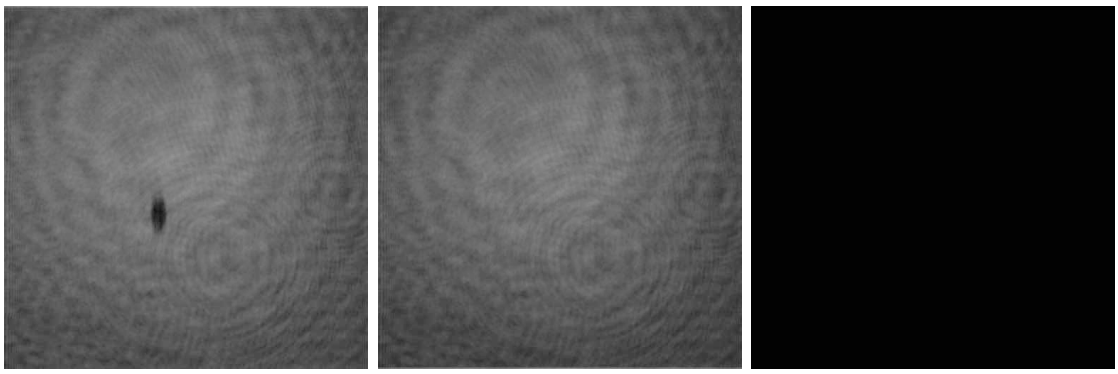

(a) I_{atom} (b) I_{beam} (c) I_{bias}

Figure 2.1: The raw images of the 76th run taken in the Lattice lab the 4th of March 2019, showing how the atom, beam and the atom bias images look. The beam bias is not shown here, as it is not possible to discern any differences between the two bias images, if the same color scale are to be used as for the atom and beam images. The light on the bias image, (c), can be hard to discern, but there is a few photons measured.

The next correction is to the assumption of the ideal two-level case. The method that builds up to Eq. (2.73) assumes the ideal two-level case, which is not necessary the case. Following the initial proposition in [15], we introduce $I_s^{\text{eff}} = \alpha^* I_s$, where alpha is a dimensionless constant, which serves to model implications such as impure light polarization, structure of the excited state and the different Zeeman sub-level populations of the degenerate ground state [15]. This also means $\sigma_0^{\text{eff}} = \sigma_0/\alpha^*$. This new α^*-parameter rewrites the optical depth to,

$$\frac{\sigma_0}{\alpha^*}\tilde{n} = \left(1 + \left(\frac{2\Delta}{\Gamma}\right)^2\right)\ln\left(\frac{I_0}{I}\right) + \frac{I_0 - I}{\alpha^* I_s} \quad \Rightarrow \tag{2.75}$$

$$\text{OD} = \sigma_0\tilde{n} = \alpha^*\left(1 + \left(\frac{2\Delta}{\Gamma}\right)^2\right)\ln\left(\frac{I_0}{I}\right) + \frac{I_0 - I}{I_s}. \tag{2.76}$$

The introduction of the α^*-parameter cannot possibly do anything to the actual density distribution and only introduce a correction to the measurements. This stems from the logical argument, that for any intensity, the amount of atoms should not change. A calibration of this can be done following the methods shown in Eq. [15] and our work regarding this is discussed in more detail in Chapter 5, where I will also expand the ideas proposed in [15].

For the correction of the scattering rate, we define a new scattering rate where the collisions are included as $\Gamma^{\text{broad}} = \beta\Gamma$, which we introduce to correct systematic discrepancies of the scattering cross section from the theoretical assumptions. This leads Eq. (2.67) to become,

$$I_s^* = \frac{\epsilon_0 \omega_0^3 \Gamma^{\text{broad}}}{12\pi c^2} = \beta I_s. \tag{2.77}$$

This saturation intensity leads to,

$$\begin{aligned} \text{OD} &= \alpha^* \left(1 + \left(\frac{2\Delta}{\Gamma}\right)^2\right) \ln\left(\frac{I_0}{I}\right) + \frac{I_0 - I}{\beta I_s} \\ &= \frac{1}{\beta}\left[\alpha\left(1 + \left(\frac{2\Delta}{\Gamma}\right)^2\right) \ln\left(\frac{I_0}{I}\right) + \frac{I_0 - I}{I_s}\right], \end{aligned} \tag{2.78}$$

where $\alpha = \alpha^*\beta$. The β parameter can then be found if there is some other property that tells us something about the OD or atom number. In Eq. (2.41), it is seen that the radius of a BEC depends on the number of BEC atoms. The radius of the BEC is independent of the imaging and therefore we now have two different ways to measure the atom number, the calibration of this parameter is seen in Chapter 6.

2.4 Measuring atomic properties

With the theoretical framework of both thermal and BEC atoms established and experimental method to measure spatial density distribution, these two things only need to come together in order to finding the different properties of the atomic clouds, e.g. atom number and sizes, by utilising,

$$\text{OD}(x, y) = \sigma_0 \int_0^\infty n(x, y, z)\, \mathrm{d}z\,. \tag{2.79}$$

For the Bose-enhanced fit, we assume $\tilde{z} \approx 1$, as this is the case at $T = T_c$ and we correct for the center of the cloud not necessary being at 0, which leads to the expression for thermal Bose-Enhanced cloud seen in Eq. (2.32) to become,

$$\text{OD}_{\text{bose}}(x, y) = \frac{N_{\text{thermal}}}{2\pi w_x w_y \zeta(3)} g_2\left[\exp\left(-\frac{(x - x_0)^2}{2w_x^2} - \frac{((y - y_0)^2}{2w_y}\right)\right], \tag{2.80}$$

where x_0 and y_0 are the center of the cloud. This expression is then ready to be fitted.

For hot thermal atoms, we assume that $\tilde{z} \ll 1$, which leads Eq. (2.32) to become,

$$\text{OD}_{MB}(x, y) = \frac{N_{thermal}}{2\pi w_x w_y} \exp\left(-\frac{(x - x_0)^2}{2w_x^2} - \frac{((y - y_0)^2}{2w_y}\right). \tag{2.81}$$

Lastly for BECs the expression in Eq. (2.40) is only for $\mu - U(\mathbf{r}) > 0$, otherwise it is zero. This can be fixed with always choosing the higher number of 0 and the expression in Eq. Eq. (2.40), this together with Eq. (2.79) yields,

$$\mathrm{OD}_{\mathrm{BEC}}(x,y) = \frac{5N_{\mathrm{BEC}}}{2\pi R_x R_y} \max\left(0, \frac{(x-x_0)^2}{R_x^2} - \frac{(y-y_0)^2}{R_y^2}\right)^{3/2}. \tag{2.82}$$

Armed with these three equations it is now possible to couple the experimental measurements from the absorption imaging together with the theory. One is almost tempted to make an evaluation program on the basis of this, just like it is seen in Chapter 4.

Chapter 3

Experimental overview

The first section of this chapter briefly describes how the experiment is producing Bose-Einstein Condensates. Some of these steps I have been involved in optimising, when this is the case I will describe that step and how it have been optimised in Section 3.3.

3.1 Experimental sequence

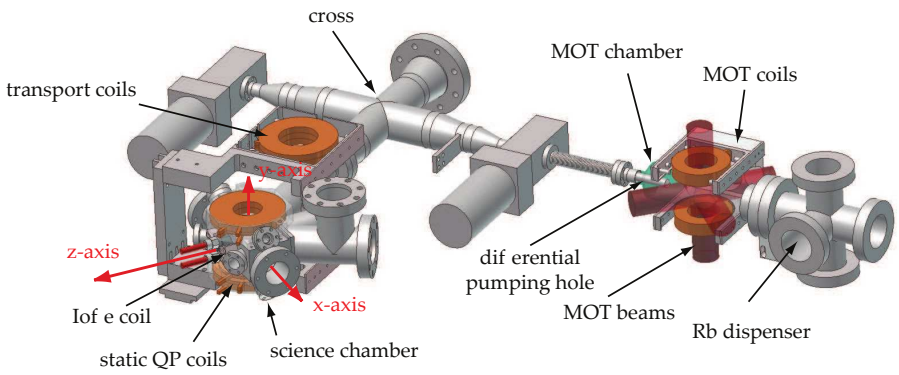

Figure 3.1: Overview of the physical experiment. Reproduced from [16].

The word "run" is used to denote one run-through of the following sequence:

1. *Magneto-optical trap (MOT)*: First the experiment loads atoms into a magneto optical trap (MOT). This is done by having a ^{87}Rb dispenser pumping out atoms at a constant rate, then these are immersed in red detuned light from all spatial directions, seen on Figure 3.1 as the 5 red beams called MOT beams, where the 6th is not visible on Fig. 3.1. This near resonant light coupled with a magnetic quadrupole field makes the atoms resonant with the light if it moves away from the center, due to the Zeeman effect. By absorbing a photon the

atom is pushed back towards the center of the trap. In order for the atom to distinguish between the pair of counter-propagating beams hitting it, the two beams are given opposite circular polarisations, so that the atom will always be pushed toward the center [16]. By having a photo detector measuring the fluorescence from the atoms confined in the trap, it is possible to a measure of the amount of atoms confined in the trap, so when the voltage on this detector reached an amount specified in the Experimental Control System (ECS), it triggers the next phase of the experiment.

2. *Optical pumping*: After the atoms are loaded and cooled, we optically pump the cloud in order to get the atoms into $|F = 2, m_F = +2\rangle$. This magnetic sub-state is trappable in the magnetic trap described in step 4.

3. *Transportation*: The moveable transport coils are turned on over the MOT chamber, creating another quadrupole field holding the atoms, while the MOT coils are turned off. The MOT chamber have an low pressure, but not low enough, as we are constantly pumping ^{87}Rb atoms into this chamber. Therefore we move the atoms into what is called the *science chamber*, where the pressure is lower. These two chamber are connected by a narrow tube, making it possible to have different pressures and transport the atoms between these different pressurised chambers.

4. *Loading in science chamber*: When the atoms are moved into the science chamber, the QUIC trap is turned on, while the quadrupole transport coils are turned off. While we are in the science chamber, we also uses 3 sets of Helmholtz coils, that we call shim coils.

5. *Evaporative cooling*: When atoms arrive in the science chamber and is transferred to the QUIC trap, we start on the evaporative cooling of the atoms. This part is the most time consuming part, taking up to a whole minute in each run. How this works and a re-optimisation can be seen in Subsection 3.3.2.

   While we are doing the evaporative cooling we are also interested in the amount of atoms trapped. Measuring the florescence as is done in the MOT does not give a very accurate measure of the atom number, as there are too many parameters influencing this. For there to be the same amount of atoms for each experiment a more accurate measurement is needed. However the imaging method used can not be absorption imaging, as this is a destructive measurement and would therefore ruin the experiment. Instead the imaging is

done by so called Faraday imaging. The Faraday imaging system was set up before I joined the work in the lab and it have worked for all the time I was in the group, therefore I will not touch the subject of how Faraday Imaging works, but for the purpose of this thesis, it is non-destructive imaging that gives an estimate of the atom number with near shot noise precision ($1/\sqrt{N}$). For greater detail it is described in [11] and [17], with mind on the actual experiment. After the first 3 steps of evaporation, a series of Faraday images are taken to get a measure of the atom number. Then we do the stabilisation, where the goal is to remove atoms until a wished atom number is reached, while not changing the temperature. If we look at the Maxwell Boltzmann distribution, the only place where we can remove atoms without changing the temperature, is at the mean velocity. This is done by finding the correct cut depth, as described in subsection 3.3.4. The cut depth decides at which energies the atoms are removed, but it does not say anything about the amount. The amount of atoms is decided by the amount of RF pulses made on the cloud and this found through feedback stabilisation, which is described in more detail in subsection 3.3.3. After the stabilisation and the next evaporation step, a new set of images are taken, this time to measure the success of the stabilisation.

6. *Hold time*: After we have evaporated down to the desired energy we hold the BEC and/or thermal cloud confined for a certain amount of time, in order to get it to rethermalise, otherwise the cloud is not in thermal equilibrium and we would not see the density profile the theory predicts.

7. *Time of flight*: Time of flight starts from the moment the trap is turned off and the atomic cloud is then falling down towards the center of Earth's gravity. However it might be worth noting that there are in fact still magnetic fields in play here, as it is only the QUIC trap that is turned off, there is still a magnetic field from our shim coils, in the case of the y- and z-shim coils it is to counter balance the natural background so the resulting field in those directions are zero. For the x field the field is not aimed at getting a resulting null-field, as we are not interested in having $\mathbf{B} = 0$, as this can make the atoms do a spin-flip, which we are not interested in and is explained in Section 3.2. After the specified time of flight the absorption images - described in section 2.3 - are taken and the data can be extracted.

3.2 Magnetic trapping

In order to be able to make a BEC in a dilute gas, we need the atoms cooled, compressed and isolated [10].The compression and isolation of the atoms is up to the trapping, while the cooling of the atoms is a job for electro-magnetic radiation. As the atoms used are without any resulting charge, there are two ways to confine them, either with an optical dipole trap or through magnetic trapping. As the title of this section suggests, the trapping method used in this thesis work is the magnetic trapping method and the optical dipole traps will not be described in this thesis.

In order to trap the atoms, a potential well of some kind is required. This can in principle be achieved by either weak-field seeking atomic states or high-field seeking states. However a theorem based on Maxwells equations state [18]: "*In a region devoid of charges and currents, the strength of a quasistatic electric or magnetic field can have local minima but not local maxima*".This implies that only weak-field seeking states that can be trapped by a magnetic field. The potential the atom feels can be described as,

$$V(\mathbf{r}) = -\boldsymbol{\mu} \cdot \mathbf{B}(\mathbf{r}), \tag{3.1}$$

where $|\boldsymbol{\mu}| = m_F g_F \mu_B$. One way to trap the atoms are through a symmetric trap, which can be delivered with one of the simplest field setups, the two-coil quadrupole trap. This trap is build by two coils with 1.25 times their radius between them [14] and with opposite running currents. It can easily be seen that in the center of the trap the magnetic field is zero. With the zero point established the rest of the trap can be described as[14],

$$B = \boldsymbol{\nabla} B \sqrt{\rho^2 + 4z^2} \tag{3.2}$$

where $\rho^2 = x^2 + y^2$. In order for the atoms to be confined and feel the right potential it requires the magnetic moments orientation to be the same with respect to the magnetic field as the atoms move, otherwise they will become ejected from the trap. This first and foremost requires the atoms to be slow enough as to ensure that the interaction between the magnetic moment and the magnetic field happens adiabatic. This is especially important if the atoms passes through an area where the magnetic field is small, leading to small separation between the Zeeman sub-levels, where these other sub-levels most likely will be untrapped or anti-trapped states. This can in essence be written as [14],

$$\left| \frac{\mathrm{d}\mathbf{B}}{\mathrm{d}t} \frac{1}{\mathbf{B}} \right| \ll \omega_L = \frac{\mu |\mathbf{B}|}{\hbar}, \tag{3.3}$$

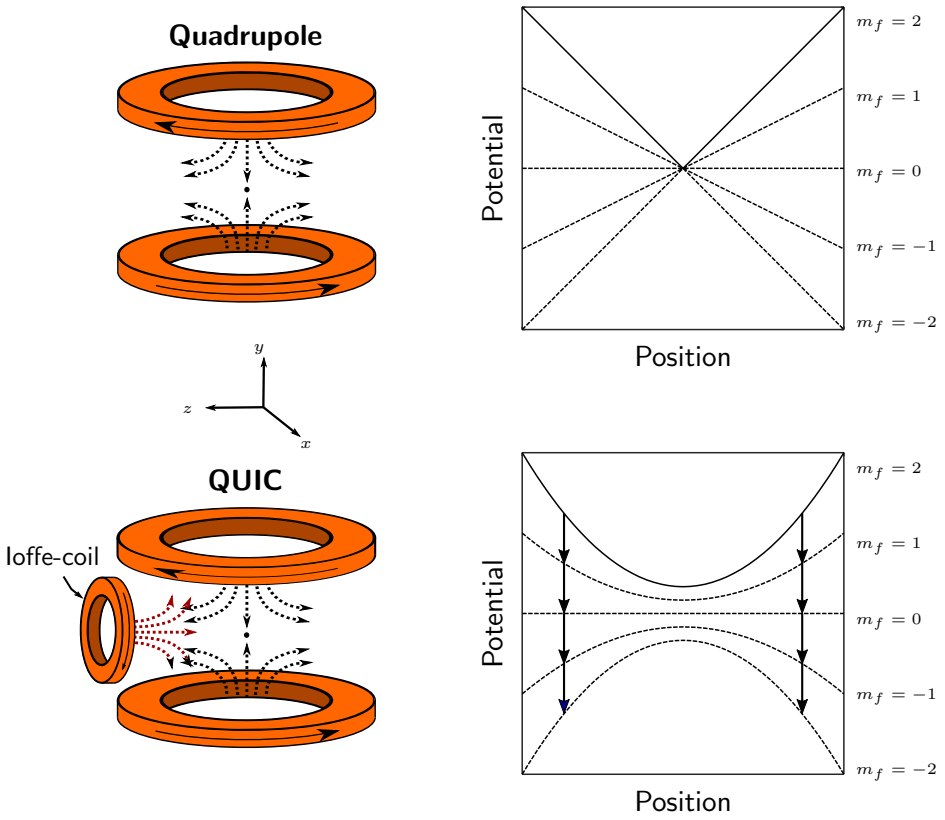

Figure 3.2: Schematic over the two different coil-setups in question. In the top we have the quadrupole trap configuration and its potential. In the lower half we have the QUIC-setup, where an Ioffe-coil have been added to make the potential have a non-zero center. The z-axis is going through the center of the Ioffe coil. Reproduced from [11].

where ω_L is the Larmor precession rate. It can easily be seen that this adiabatic condition is violated in regions with a very small magnetic field, especially if $|\mathbf{B}| \to 0$. This introduces a hole in the trap where the atomic spin might flip, called *Majorana spin flip* [14]. In the production of BEC, this is problematic as it is the atoms with the lowest energy we are interested in and these are spatially around the zero point.

Therefore another trap is required. There are a number of solutions to this, but the one used in the work of this thesis is the Quadrupole Ioffe Configuration (QUIC) trap. This trap consists of a quadrupole coil pair with an additional third coil called the Ioffe coil, as can be seen on Fig. 3.2.

The QUIC trap is in essence a trap with tries to emulate the Ioffe-Pritchard trap. For all intents and purposes the QUIC trap can be described with the same magnetic

field as the Ioffe-Pritchard trap, which is given as [10],

$$\mathbf{B} = B_0 \begin{pmatrix} 0 \\ 0 \\ 1 \end{pmatrix} + B' \begin{pmatrix} x \\ -y \\ 0 \end{pmatrix} + \frac{B''}{2} \begin{pmatrix} -xy \\ -yz \\ z^2 - \frac{1}{2}(x^2+y^2) \end{pmatrix}. \tag{3.4}$$

This means the field strength of the magnetic field is given as,

$$|\mathbf{B}(\mathbf{r})| = \sqrt{\left(B'x - \frac{B'}{2}xz\right)^2 + \left(-B'y - \frac{B''}{2}yz\right)^2 + \left(B_0 + \frac{B''}{2}z^2 - \frac{B''}{4}(x^2+y^2)\right)^2}. \tag{3.5}$$

This trap solves the problem with spin flips, by having a non-zero magnetic field everywhere. That this is zero everywhere is perhaps not trivial and it depends on the values of B_0, B' and B''. One argument for it being non-zero everywhere, can be seen by considering the point $\mathbf{r} = (0,0,0)$ where $|\mathbf{B}| \neq 0$. By going back to the previous statement about no local maxima in a region devoid of charges and currents, we can then see if we somehow can get a magnetic that is lower by going in any direction. If the magnetic field rises in all directions, then there would have to be maximum If we make a small change in any direction and this increases the magnetic field, then for a point where the magnetic field is lower than $\mathbf{r} = (0,0,0)$ to exist, will require a local maxima and that cannot exist.

From Eq. (3.5) we can see if $B'(r_{x,y} - r_{x,y}z/2) \gg B''r_{x,y}^2$ is the case, then $\mathbf{r} = (0,0,0)$ is the trap minimum. for small perturbations this is always the case, as we are talking small perturbations to the spatial coordinates, making $r_i \gg r_i r_j$. As our trap is measured in µm, this means in the radial directions, the linear confinement is stronger than the harmonic component, while the axial direction (z) is only trapped by the harmonic component, leading to a prolated trap. This can be taken one step further, where the bias field is also ignored, as it is only the change in position that we are interested in,

$$|\mathbf{B}(\mathbf{r})| \approx \sqrt{(B'\rho)^2 + \left(\frac{B''}{2}\right)^2 z^4}. \tag{3.6}$$

In the limit of a cold cloud, we can then use the standard binomial approximation $(1+x)^n \approx (1+nx)$ for small x,

$$|\mathbf{B}| \approx B_0 + \frac{\rho^2}{2}\left(\frac{B'^2}{B_0} - \frac{B''}{2}\right) + \frac{B''}{2}z^2. \tag{3.7}$$

Recalling equation (3.1) and then recognising that this is a harmonic oscillator, the potential can be written as,

$$U(\mathbf{r}) = \mu B_0 + \frac{1}{2}m\omega_\rho^2\rho^2 + \frac{1}{2}m\omega_z^2 z^2, \tag{3.8}$$

where m is the mass of the atom in question, and

$$\omega_\rho^2 = \frac{\mu}{m}\left(\frac{B'^2}{B_0} - \frac{B''}{2}\right) \quad \text{and} \quad \omega_z^2 = \frac{\mu}{m}B''. \tag{3.9}$$

From this it can be seen that if the bias field in the z-axis is increased, then the radial frequencies will change but the axial will remain unchanged.

3.2.1 Decay of the magnetic field

Ordinarily in BEC experiments measurements are taken after time of flight, which means the trap needs to be turned off. But it is not possible to turn off a current instantaneously. The decay of the current can be determined starting from Faraday's law [19],

$$\mathcal{E} = -\frac{\mathrm{d}\Phi}{\mathrm{d}t}, \tag{3.10}$$

where $\mathcal{E}$ is the electromotive force and can be rewritten as $\mathcal{E} = RI$, and Φ is the flux. Under the assumption of magnetostatics (which holds throughout the turn-off under the assumption of quasistatic currents) the magnetic field is given as [19],

$$\mathbf{B}(\mathbf{r}) = \frac{\mu_0}{4\pi} I \oint \frac{\mathrm{d}\mathbf{I} \times \hat{\mathbf{r}}}{\mathbf{r}^2}, \tag{3.11}$$

which says that the magnetic field from any part of the coil is directly proportional to the current. This implies that, the magnetic flux, Φ, is also directly proportional to the current, and enables us to define $\Phi = LI$, where L is the inductance of the coil. Thus we can rewrite equation (3.10) as,

$$RI = L\frac{\mathrm{d}I}{\mathrm{d}t} \Rightarrow \frac{R}{L}\mathrm{d}t = \frac{1}{I}\mathrm{d}I \Rightarrow I(t) = I_0 e^{-\frac{R}{L}t} = I_0 e^{-t/\tau}, \tag{3.12}$$

given the proportionality between the magnetic field and current, this means the magnetic field decays exponentially when the trap is turned off.

3.3 Maintenance measurements

Some parameters change over time and needs to be measured and readjusted from time to time, in this section I will explain more in-depth some of this maintenance measurements I have worked on.

3.3.1 Life time

At the beginning of my time on the Lattice experiment we experienced trouble with the atom numbers in our trap being a lot lower than expected. This was due to

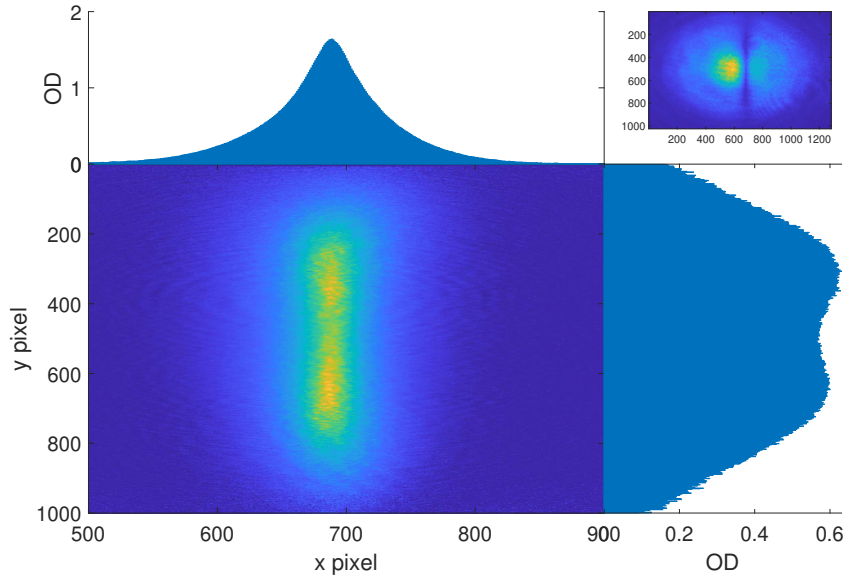

Figure 3.3: Picture of a atomic cloud with two minima, with each of its two axes integrated and shown on the sides. The small image in the upper right corner is the shadow picture, where it can be seen that the atoms cast a shadow in the laser beam, seen from the camera. This image is taken at a early state of the evaporation and in-trap with our secondary camera.

our trap having not one, but two points where the magnetic field was zero leading to Majorana spin flips, an image from that time is seen on Figure 3.3. This led us to investigate the lifetime for different bias fields. This was investigated for a huge thermal cloud without stabilisation. The images are taken in-trap after the first few evaporation steps. These measurements are taken by simply varying the hold time and then fitting to an exponential decay, this is then done with a magnetic field of $I_{zShim} = -0.136\,71\,\mathrm{A}$ and again for $I_{zShim} = 2\,\mathrm{A}$. The idea behind this investigation is, if somehow we have a negative magnetic at the center, we would also have two point where $|\mathbf{B}| = 0$, by increasing the shim current, we increase the magnetic bias field and would no longer have a magnetic zero point. The result of this investigation can be seen on Fig. 3.4.

It can then clearly be seen on Fig. 3.4, that whether the field have two magnetic null point or none, makes a difference. We can therefore conclude that atoms are leaving the trap more rapidly if we have two holes in the trap, which is consistent with our expectation from Section 3.2.

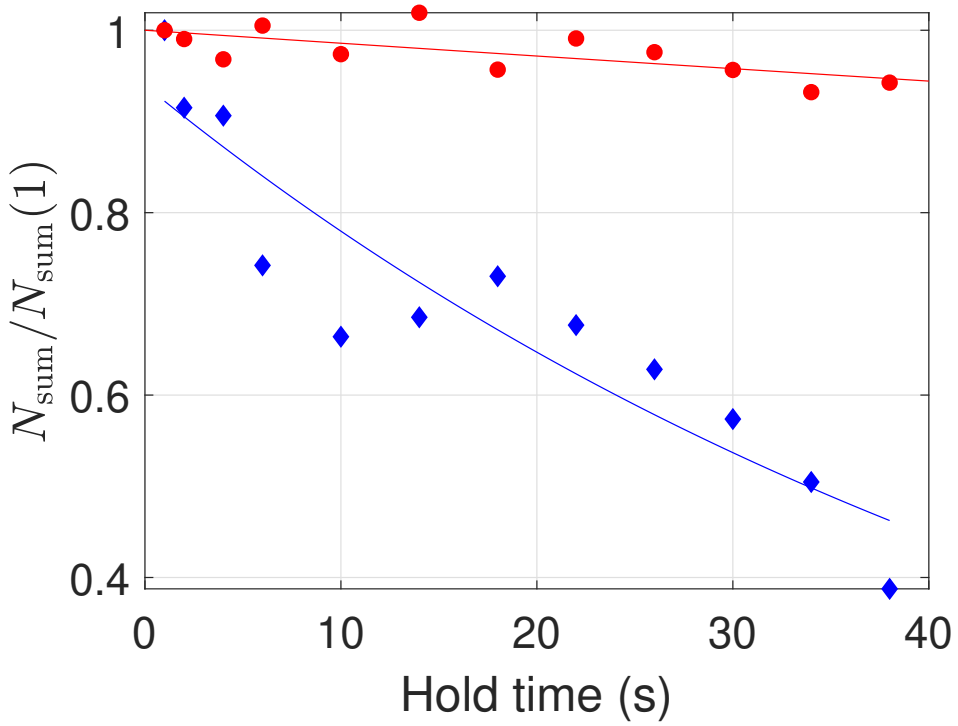

Figure 3.4: The decay of the normalised atom number in the QUIC trap with $I_{\mathrm{shim}}, z = -0.136\,71\,\mathrm{A}$(◆) and $I_{\mathrm{shim}}, z = 2\,\mathrm{A}$(●), giving lifetimes of $\tau = 53(16)\,\mathrm{s}$ and $\tau = 697(519)\,\mathrm{s}$, respectively. Each data point is one measurement. Note that these lifetimes are for a thermal cloud without any evaporation and therefore only reflect the natural decay. Each data point holds only one measurement.

3.3.2 Evaporative ramp

In order to achieve Bose-Einstein condensates, it is important to have an effective cooling, for this we use evaporative cooling in the Lattice laboratory. The overall goal that evaporative cooling have to satisfy is to get as many atoms as possible with the lowest temperature possible. This is a bit tricky, as the general idea of evaporative cooling is to remove the most energetic atoms in order to lower the temperature, which means the more atoms, the higher temperature. But we can quantify the requirement by using phase-space density, seen in Eq. (2.7), reproduced here,

$$\rho_{ps} = n\lambda_{dB}^3 = n\left(\frac{2\pi\hbar^2}{mk_bT}\right)^{3/2} \tag{3.13}$$

where n is the particle density, m is the mass of the atom and λ_{dB} is the de Broglie wavelength. Doing most of the evaporation the atoms have not made the transition to a BEC, therefore this description is adequate. By utilising the kinetic energy from the temperature of the cloud is equal to the confinement at the edge of the cloud,

the volume can be written as,

$$V = \left(\frac{2\pi k_b T}{m}\right)^{3/2} \frac{1}{\omega_x \omega_y \omega_z}, \tag{3.14}$$

which means we can describe the phase space density as,

$$\rho = N\hbar^3 \frac{\omega_x \omega_y \omega_z}{(k_b T)^3}, \tag{3.15}$$

which is then a measurable quantity, as both the atom number, N, and temperature, T, are measurable quantities.

As it was established in equation (3.8), the potential of the atoms is an harmonic oscillator, then imagine some thermal atoms in this potential, as is schematically shown on Fig. 3.5. A sort of cartoonish way to understand this is, if one makes a "hole" in the potential, then only atoms with that energy corresponding to the hole can escape the trap. Then if we then move this "hole" down, we will keep removing atoms. Physically what happens, is an utilisation of the Zeeman splitting, where the atoms with the highest energy is able to reach farther out, where the field is higher, this also means their resonance frequency also will be a bit higher making it possible to tune a radio frequency source to resonate with the atoms and then making then change from the bound $|F = 2, m_F = 2\rangle$ to $|F = 2, m_F = -2\rangle$ which is repelled from the trap minimum [9].

If we just remove all atoms too energetic, it does not cool down the rest of the atoms, which is what is wanted in the end. As previously stated, the atoms during most of the evaporative cooling can be regarded as thermal atoms, and thus we can describe the atoms with Maxwell Boltzmann statistics, the idea is to remove the tail of the Maxwell-Boltzmann distribution and then let the cloud rethermalise through collisions. This is done in a number of steps, until the desired temperature is reached. Each step have a chosen RF frequency and an associated time, generally the more time, the higher phase space density. However there are of course also some loss mechanisms, like collisions with the background, inelastic and three-body collisions, which means the desired time is an optimum between good evaporation and loss. For an experimental realisation this means we have to find the optimal trade-off between atom number and phase space density, which is not necessary straightforward, but an example can be seen on Figure 3.6. Here the evaporation frequency was constant and the time of which this evaporation was made over was varied, in order to find the time that best matches the chosen frequency, 4.5 s was chosen as the best as it shows a good combination of phase space density and atom number. 5.5 s could also have been chosen. By doing this for all steps but the last, as this one we change the

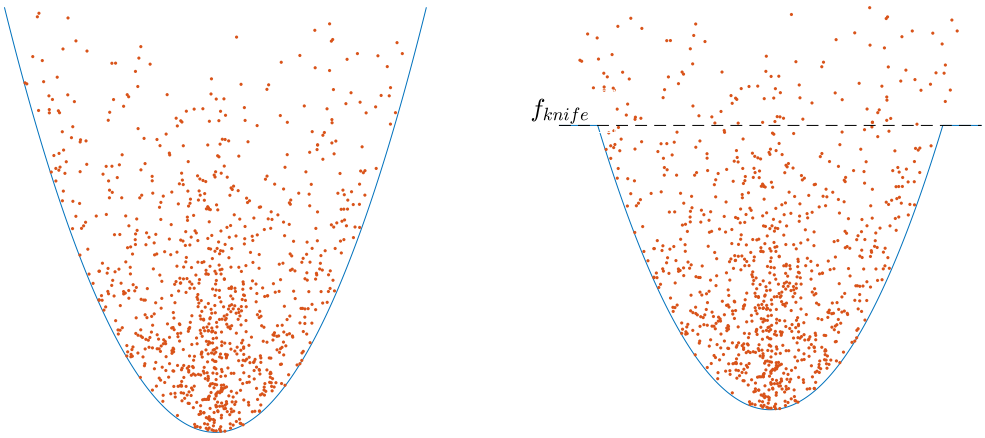

(a) (b)

Figure 3.5: The idea behind evaporation cooling. Dots represent atoms.(a) natural potential around the center of the QUIC trap. (b) The potential but with a radio frequency knife utilised, effectively lowering the trap. If done correctly, all atoms above f_{knife} is no longer bound in the trap as they are in untrapped or antitrapped states and thus no longer confined the magnetic field.

last very often in order to control the final temperature therefore an optimisation is redundant. We therefore arrive at Figure 3.7, which shows how our RF frequency changes over time.

3.3.3 Feedback stabilisation

The Lattice experiment uses atom stabilisation, this requires feedback stabilisation now and then. This is something that is done quite often, when the experiment is running optimally it is usually done once a week at the least. The purpose of the feedback stabilisation is in the end to ensure that the correct amount of atoms are in the trap after a given evaporation step (usually the fourth). This is done by applying RF pulses that remove atoms with the mean velocity, but as this mean velocity is already found (see subsection 3.3.4), the purpose of feedback stabilisation is in more practically terms, to find how many pulses are needed to achieve the correct atom number. This is done by first taking a set of runs for reference, this is the so called reference runs. These reference runs have not been exposed to any loss pulses, they therefore represent the natural spread of atom numbers. Then from the reference runs and the run that we wish to stabilise, a quantity we call error is calculated as [11];

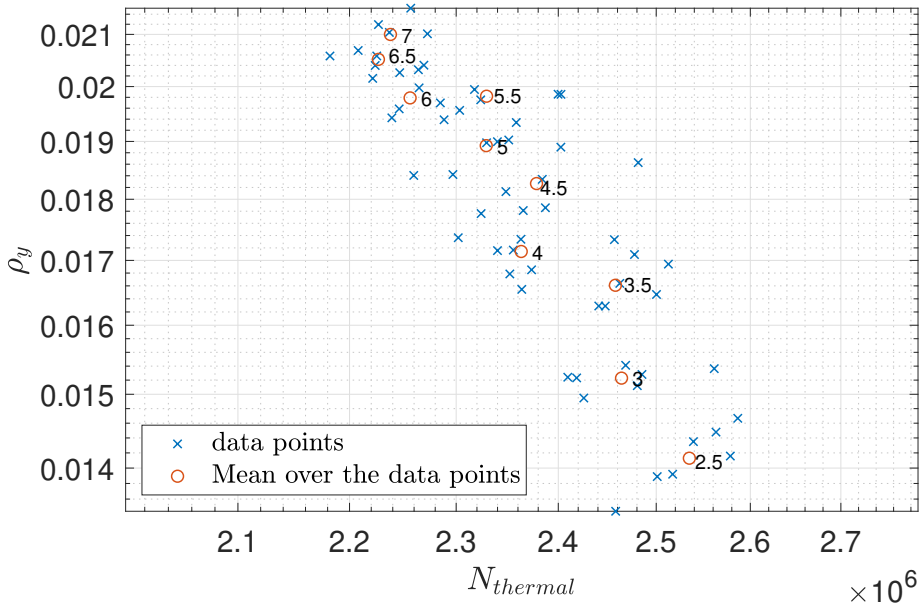

Figure 3.6: The amount of (fitted) thermal atoms versus Phase space density in the y direction, this is directional as the found temperature from the evaluations is not necessarily the same in both directions, see section 4. The numbers denote the time associated with every mean time. 4.5 s is the chosen value here.

$$E_1^{\mathrm{REF}} = \frac{S_{F1}}{\langle S_{F1}^{\mathrm{REF}} \rangle} - 1 \quad \text{and} \quad E_2^{\mathrm{REF}} = \frac{S_{F2}}{\langle S_{F2}^{\mathrm{REF}} \rangle} - 1, \tag{3.16}$$

where S is the signal, the subscript denotes if it is before the stabilisation, $F1$, or after, $F2$. The loss of the atoms should follow the amount of pulses exponentially [11]. However, due to technical limitations we are approximating it with a quadratic polynomial[11],

$$N_{\mathrm{pulses}} = gE_1^{\mathrm{REF}}(1 + qE_1^{\mathrm{REF}}) + d_{\mathrm{pulses}}, \tag{3.17}$$

where g and q are the linear and quadratic gain terms, respectively. d_{pulses} is the loss at $E_1^{\mathrm{REF}} = 0$ also known as where the stabilised signal is equal to the mean of the signals from the reference runs. These feedback parameters are often chosen through an iterative process, by putting in a guess for these parameters some atoms will be removed according to equation (3.17), however the aim is to get E_2^{REF} to lie on a horizontal line, for all runs, and thus stabilising the error, which means the atom number is stabilised. An example of a feedback calibration can be seen on Fig. 3.8, on this figure, the signal of the points with loss clearly follows another trend than the reference runs, however the signal - and therefore also the atom number - is not stable from run to run. However we have an evaluation program which are able to predict what parameters are better in order to achieve the target E_2^{REF} wanted, this

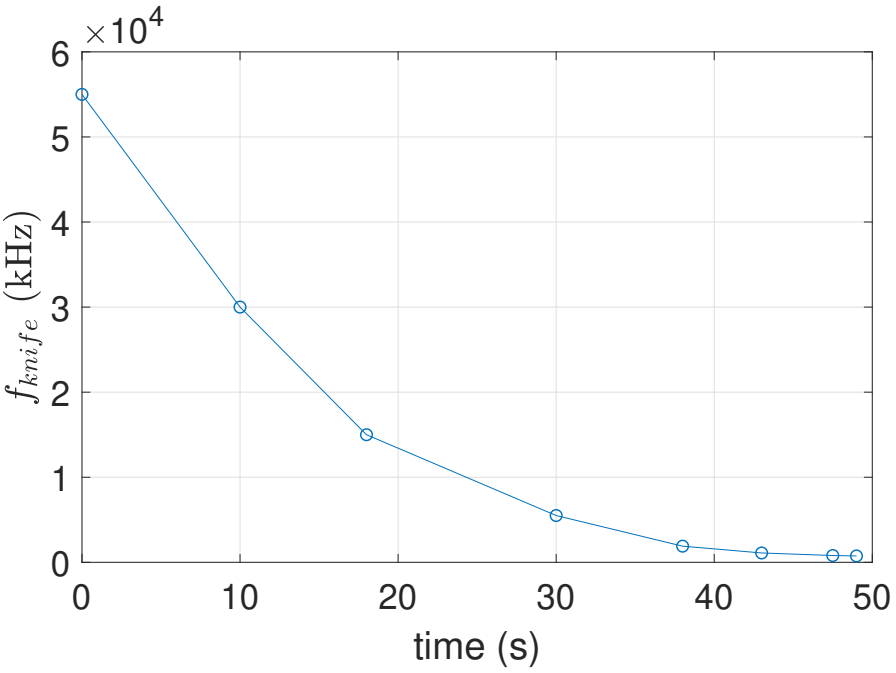

Figure 3.7: Evaporation ramp for the experiment.

is the black line shown on Fig. 3.8.

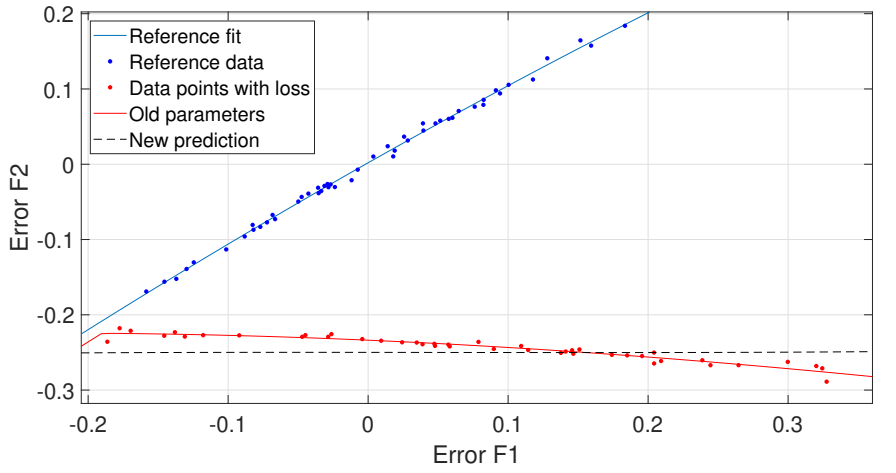

Figure 3.8: An example of how Feedback stabilisation is made, the ideal case is if stabilised points lie on a horizontal line. Reference runs are from the 20th of March, 2019 and the stabilised points are from the 21th of March 2019.

3.3.4 Cut depth

When doing atom number stabilisation it is desirable to change only the atom number without influencing the temperature. For a thermal cloud, the energy distribution of the atoms is given by the Maxwell-Boltzmann distribution. By removing the most energetic atoms, the cloud will cool down, while removing the least energetic

atoms will of course heat up the cloud after a rethermalisation. If we remove the atoms with the mean energy, the temperature will remain unchanged. We thus need to determine the appropriate radio frequency for the loss that achieve this. This frequency is between the evaporation frequency f_{knife} and the trap bottom f_{bottom} and can be specified through a cut depth, D, given by,

$$f_{\langle E \rangle} = D(f_{\text{knife}} - f_{\text{bottom}}), \tag{3.18}$$

where D is a number between 0 and 1. The cut depth can be determined, by using the property that only for the correct value of D the temperature of the sample is independent of the induced loss during feedback. By using equation (3.17)'s d_{pulses} and set $g = q = 0$, it is possible to change the amount of lost atoms for each cut depth easily. This is shown in Fig. 3.9, where a 1st order polynomial fit have been applied to the temperature as a function of the lost fraction. The goal is then to find the fit where there is no slope. By fitting a spline to the slope as a function of cut depth the zero-crossing corresponding to the optimal cut depth is found to be $D = 0.085$.

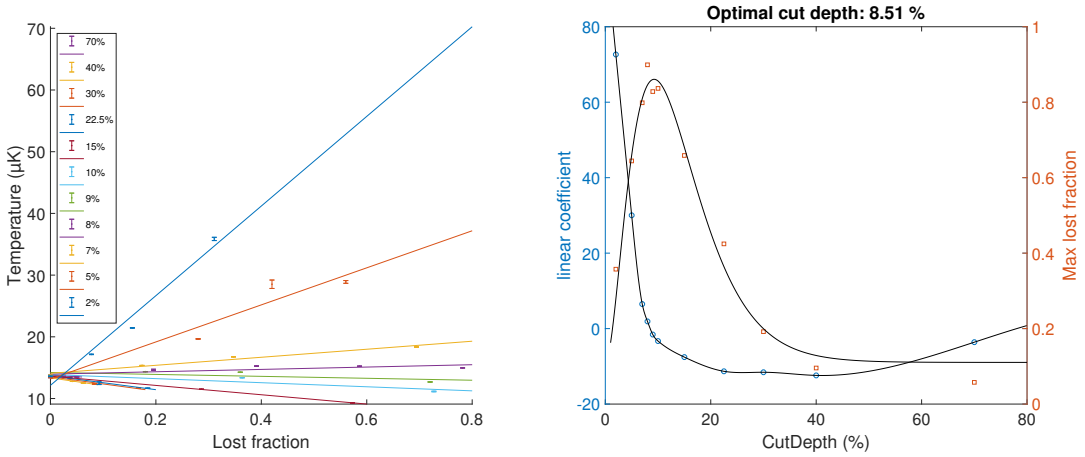

(a) (b)

Figure 3.9: Result from the cut depth investigation. (a) The temperature as a function of how large a fraction of the atoms have been lost, fitted to a first order polynomial, for different cut depths. Each data point consists of at least 3 runs. (b) Left axis: The blue circles denote the linear coefficients from (a) for each investigated cut depth. A spline function have been used to determine where the coefficient is zero and the temperature is unchanged. Right axis: The red squares denotes the max fraction that can be removed. This is fitted to a Maxwell-Boltzmann distribution and are shown as a sanity check and illustrate that the more atoms we are resonant with, the higher loss we induce.

3.3.5 Trap frequencies

As was seen in Eq. (3.8), the trap frequency stems from Hooke's law and tells us how tight the trap confines the atomic cloud. This means the width of the cloud before the magnetic field is turned off, depends on these frequencies, it can therefore be important to know what trap frequencies the cloud experiences.

The trap frequencies can be measured by giving the cloud a "kick" that makes the cloud move in the trap, given that the magnetic field from the QUIC-trap is harmonic around the minimum point, we expect it to move like an harmonic oscillator. By holding the cloud for variable time duration before it is released into time of flight, we can measure the periodicity of its in-trap oscillations, by seeing it moving sinusoidal in both directions of the picture.

In my time on the experiment this "kick" have been initiated in a number of ways. This "kick" needs to be strong enough to make the atoms oscillate in both directions with an amplitude, large enough to be clearly distinguishable, which proved to be a challenge.

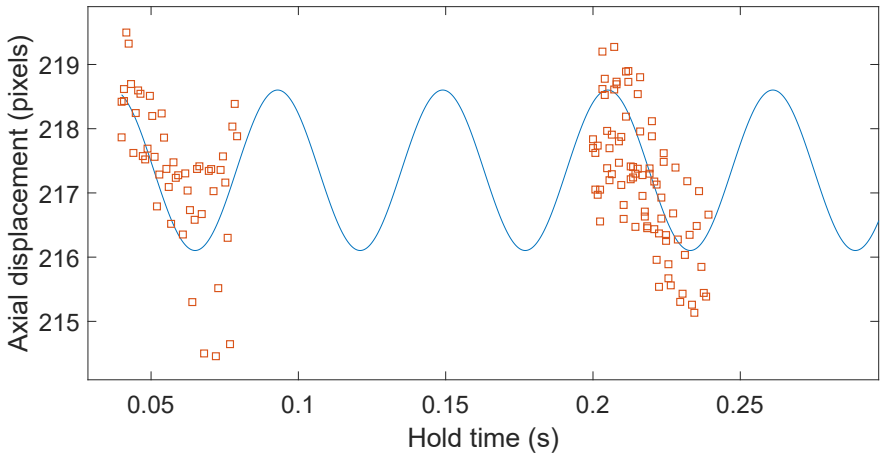

Figure 3.10: Displacement of the center of a BEC under trap frequency measurement, where the oscillation is started by lowering the QUIC current in short period of time. Each point represent one run. Note, there are more runs with the same hold time.

Perhaps the simplest way to start the "kick" is to just ramp the shim coils up for a short time, thus changing the position of the minimum point. This works great for the radial direction, but it proved hard do a good oscillation in the axial z-direction. We had a bit more success with ramping the QUIC current down for a short time, but this had small oscillations in the axial direction of about 3-5 pixels, which makes it possible to observe an oscillation, but hard to get a good measure of, making the

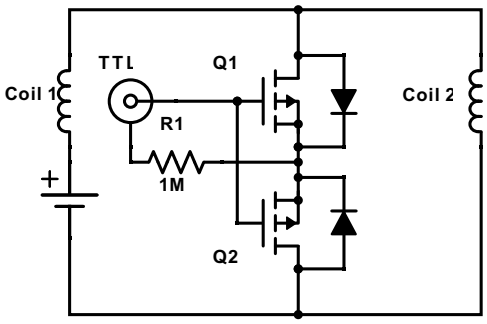

Figure 3.11: Schematic of the little circuit built in order to Bypass one of the quadrupole coils in or z-shim coil. The diodes are built into the MOSFETs. The TTL is a digital channel we can control from the Experimental Control System (ECS).

fit rather hard, as can be seen on Figure 3.10, where the trap frequency is estimated to $\omega_a = 2\pi \times 17.85(19)\,\text{Hz}$.

The last method, which also proved to be the best, was to bypass one of the quadrupole coils in our z-shim configuration. This was experimentally done, by constructing the circuit seen on Fig. 3.11 and then when we want to start the oscillation, we send a 5V signal through to TTL and thus closing both MOSFETs so that the current can run through the MOSFETs. We build the circuit seen on Fig. 3.11 with two MOSFETs as this system also should be able to handle negative current and the built-in diodes in these MOSFETs were the diodes with the lowest resistance we could find. And the resistance needs to be low for there to run a considerable current through the bypass, as Coil 2 have a resistance of $\sim 1.2\Omega$.

The result of a oscillation with this bypass can be seen on Figure 3.12, this have clearly improved our trap measurement capabilities, as we can now be more certain of the fit than before and have yielded $\omega_a = 2\pi \times 17.72(1)\,\text{Hz}$ it have lowered the uncertainty by a whole order of magnitude.

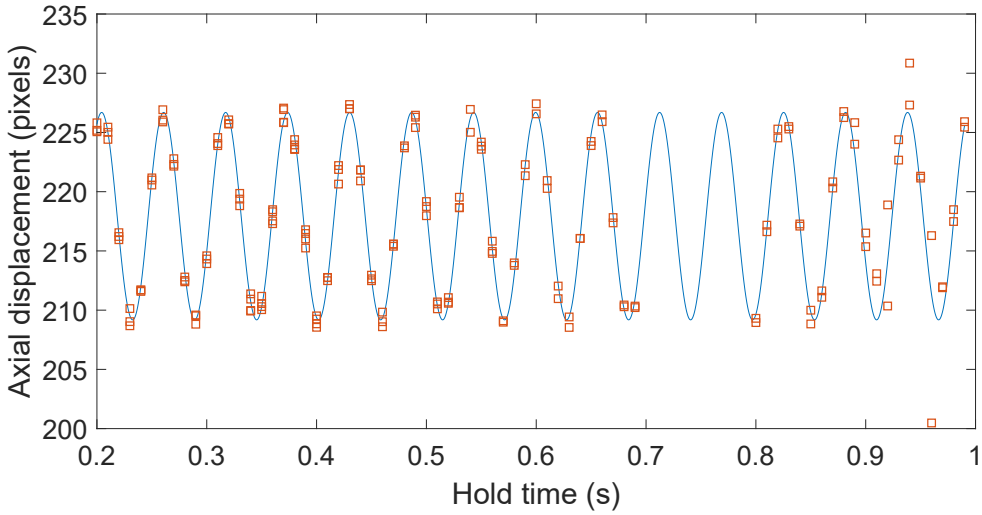

Figure 3.12: Displacement of the center of a BEC under trap frequency measurement, with the oscillation started by bypassing one of the shim coils. Each point represent one run. Note, there are more runs with the same hold time.

Chapter 4

Evaluation program, SkyFit

This code is made with the goal to be able to evaluate absorption imaging pictures of Bose-Einstein Condensates. SkyFit was developed with a few goals in mind. First and foremost it was to replace the old program "Perfectfit".

The goal behind this replacement was to get a code that was more up-to-date with the tools provided by Matlab and to do 2D evaluations of the images, where Perfectfit only did 1D fits. Another goal that was quickly set for SkyFit was also to put the three associated laboratories onto the same program. Previously, all three laboratories had their own version of Perfectfit, and if one laboratory wanted implement improvements of the program, it would not be easily transferred to the other laboratories. During development, a few new features was also thought off, some of them in order to be more precise with the evaluations, other because it would make the day-to-day work in the laboratories easier. Lastly SkyFit was also meant to be an easily editable program, such that if someone thought of a new feature or simply only wanted a part of the code, a new developer should be able to implement these features somewhat easily.

This chapter is mostly based on what SkyFit will do in an "ordinary" run, i.e. a run with a good amount of thermal and BEC atoms, as this described the most general case. In the event of a run with only thermal or BEC atoms all parts containing the other can simply be disregarded, as both parts are somewhat independent.

An image of the Graphical User Interface for SkyFit after an evaluation can be seen on Fig. 4.1, with many of its possible settings seen. The settings that are not shown are general settings, like the camera and experimental parameters, that you usually do not wish to change very often.

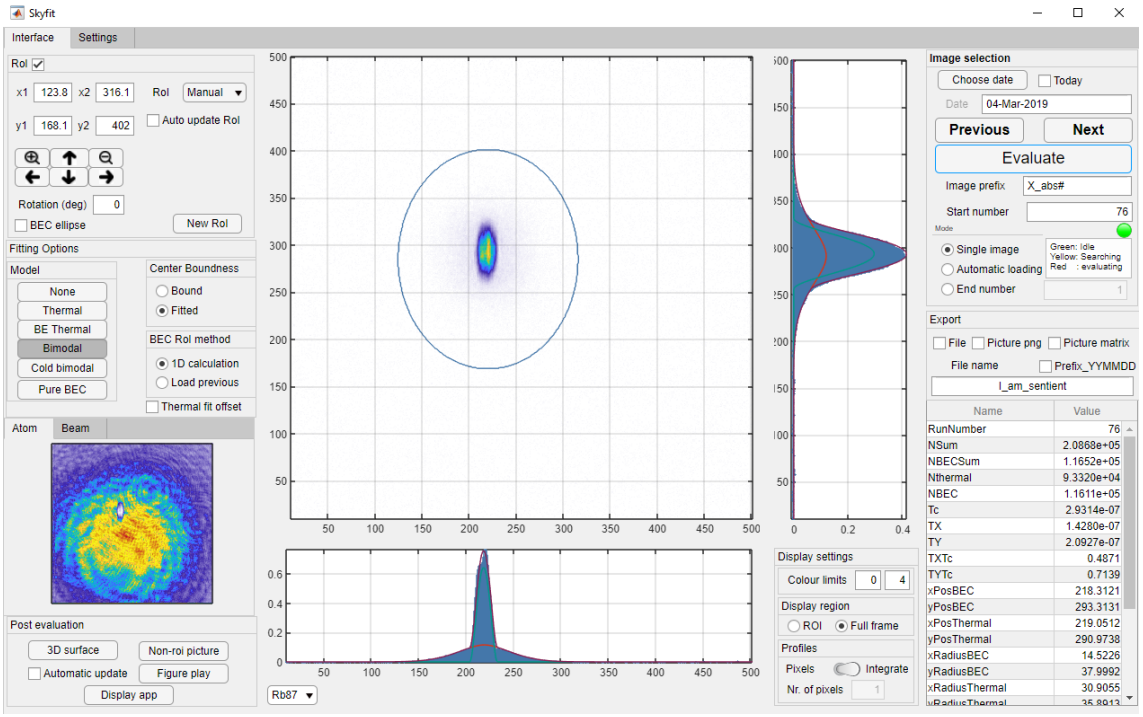

Figure 4.1: An image of SkyFit after an evaluation. It can be seen there are quite a few bottoms and check boxes. Only the ones with physic relevance will be explained. In short the settings tab that can be seen in the upper left corner is not shown here, but it contains all settings related to parameters that are dependant on the camera and the actually experimental set up (like camera calibration, time of flight and trap frequencies). On the page shown here, the top of the left "column" is where all the evaluation options are shown. Below these options, the raw atom and beam images can be switched between which one a want to see, which are the same images as seen in Fig. 2.1. The upper right "column" is where it is specified which image to load. The large image in the middle shows the OD at the different pixels, where the blue circle in the image shows the edge of the cloud RoI, this is an evaluation of Fig. 2.1. This image is flanked by by an integration of this image in the two directions, where the red curve shows the thermal fit, the green the BEC and the purple show the sum of these two.

4.1 Image loading

The first thing to do in order to evaluate an image is of course to load the image. However, defining the OD as was stated in Section 2.3, we are waiting for till later, as we need the define the Regions of Interest first, for reasons that will become obvious.

Based on Sec. 2.3, $I(x,y)$ and $I_0(x,y)$ are found by using the signal on each pixel, through,

$$I(x,y) = C_{cam}\frac{S_{atom}(x,y) - S_{bias}(x,y)}{t_{detection}}, \quad I_0(x,y) = C_{cam}\frac{S_{beam}(x,y) - S_{bias}(x,y)}{t_{detection}}, \tag{4.1}$$

where the S denote the signal in pixel x, y in the given image, which corresponds to the amount of counts in the image. $t_{detection}$ is the detection time, this is important as an image is integrated over the time it takes to take the image. Lastly, C_{cam} is what we call the camera calibration, which is a calibrated quantity that makes it possible to translate the amount of counts in a pixel to intensity and has units of $[C_{cam}] = I_s \cdot \mu s/\text{counts}$, which also means all intensities in this chapter are already divided with I_s.

4.2 Region of interest (RoI)

Before anything can be done, a user needs to define a number of region of interest to work with. These are the BEC-, thermal-, cloud- and reference-RoIs, which can be seen on Fig. 4.2. This section explains how to find these.

4.2.1 Cloud RoI

The first RoI that we need to find, is the cloud RoI. This can be found in two ways, either through the "Manual" method, where the user simply defines the RoI by using Matlabs built-in "Imellipse" function, that lets the user define an ellipse by hand. The other way to define the Cloud-RoI is by using the "Auto" method. This method normalises the picture to the maximum value found inside the Cloud-RoI from the two intensities as,

$$\text{od}_{\text{norm}}(x,y) = \ln\left(\frac{I_0(x,y)}{I(x,y)}\right)\frac{1}{\max\left(\ln\left(\frac{I_0(x,y)}{I(x,y)}\right)\right)}. \tag{4.2}$$

Then SkyFit finds the center by using a threshold value, all values above this is used to find a center. This is done by making a mask consisting of all pixels with a

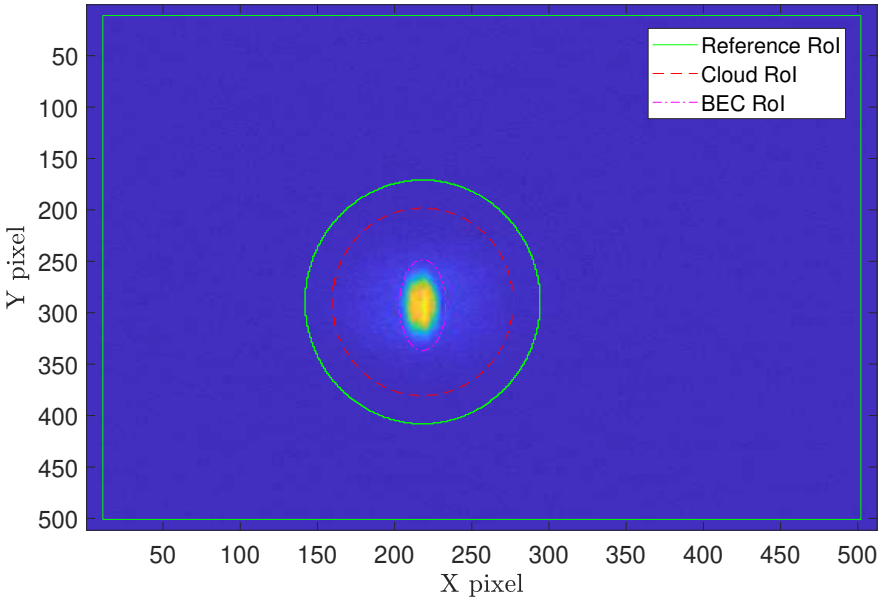

Figure 4.2: Figure of an evaluated atomic cloud with a BEC, the magenta dash-dotted line shows the bounds of the BEC RoI. The red dashed line shows the bounds of the Cloud RoI. Everything outside of the green ring and inside of the green square is the reference RoI. This is the evaluation of Figure 2.1.

normalised OD higher than the threshold,

$$M(x, y) = \mathrm{od}_{norm}(x, y) > \text{threshold}. \tag{4.3}$$

The mask is then a 2D logical array that is 1 in each pixel with an normalized OD higher than the threshold and 0 if it is not.

When looking for the center, the interesting point is the pixel in which the center is located, so the goal is the find the x and y positions of the center. This is calculated as the center-of-mass of the image by,

$$x_{center} = \frac{\Sigma\, x(M)\mathrm{od}_{\mathrm{norm}}(M)}{\Sigma\, \mathrm{od}_{\mathrm{norm}}(M)}. \tag{4.4}$$

The same is then done in the y-direction.

After finding the center there are two options, either a user can define a fixed radius, where a radius in both the x- and y-directions are chosen and the RoI is found by the center and these numbers. The other options is to calculate the radius. For this solution Eq. (4.3) is used again, but with a somewhat arbitrary threshold of 0.1, where everything above is calculated as being pixels containing atoms. This is of course dependant on the signal to noise ratio in the picture, but for most images this should be okay. The cloud is most often an ellipse, but the mean radius can be

found using,

$$r = \sqrt{\frac{A}{\pi}} = \sqrt{\frac{\sum_{x,y} M(x,y)}{\pi}}, \tag{4.5}$$

where A is the area. A and r are in units of pixels. Then the ratio between the two axes of the ellipse is found,

$$\epsilon = \frac{\text{mean}(|X - x_{center}|)}{\text{mean}(|Y - y_{center}|)}, \tag{4.6}$$

where X and Y are all x and y pixels that are inside the mask ($M(X,Y) = 1$). Then the radius in both the x- and y-direction are found,

$$r_x = x_{center} + r\epsilon, \quad r_y = y_{center} + \frac{r}{\epsilon}, \tag{4.7}$$

with these values known, an ellipse can be created and the cloud RoI defined through the "auto" method.

By finding the radii of the RoI through the auto method, the radii can differ from image to image and it can depend on what type of cloud is investigated, as a thermal cloud ordinary would have a lower OD. This is why fixed radii can be useful, under the right circumstances.

When the cloud RoI is defined we can also define what we call the "reference" RoI, which is confined by an inner radius of $R_{\text{refRoI}} = 1.3R_{\text{cloudRoI}}$ and the edges of the image. This RoI is made with the goal of having no atoms in it and thus only background. The reason why we define this RoI becomes obvious in Section 4.3.

4.2.2 BEC and thermal RoIs

With the general region of interest defined, the next thing is to define in which pixels the BEC is located. In Section 4.4 we wish to fit the part of the cloud that only includes thermal atoms and no BEC atoms. In order to do this we define two regions of interest, a BEC RoI, which define where the BEC atoms are and a thermal RoI, defining where there are no BEC atoms. This is done by finding the BEC RoI, as both of these RoIs are defined from where the BEC atoms are.

Again there are two solutions, the first is simply to use the same BEC RoI as was used in the previous run. The other solution is by making a 1D fit to the density, in order to find the width of the BEC. First, the center of the cloud is to be found. It is important that this value is precise, as the BEC is approximately symmetric around the x- and y-axes. As this is important a good start guess can be important. This is done by making a Gaussian fit;

$$f(x) = A_g e^{-\frac{(x-x_c)^2}{2c^2}}, \tag{4.8}$$

where A_g is the amplitude, x_c is the center point and c is a measure for the width of the Gaussian. It is only the center, x_c that is interesting here. This fit is of course not a good fit to the data if there are BEC atoms present as is the case here, otherwise we would not make a BEC RoI. However it does not have to as it is only the center that we wish to find. Other methods might have been used, but this method seems more robust to noise.

The BEC RoI is defined by making a combined Gaussian and Thomas Fermi fit. But in this fit it is preferable if noise plays a small part as possible, but we also want to be able to see the structure, we therefore take a 3 pixel mean around each axis that crosses the previously established center. This means there is a cross in the picture where the two axes are 3 pixels wide and meet in the center. This could in principle be higher than 3 pixels, but we let it stay here as to still be able to distinguish the BEC and if a single pixel is extremely high because of some fault in the imaging, then it might not diverge the fit as much.

Worth noting is also that the program is made with a max OD setting, which means ODs of higher than this amount (often set to 4.5) will not be a data point in this fit or any other fit.

As an example of mean method, Figure 4.3 shows three different pixel amounts for the same cloud under 10 ms of time of flight. As it is seen the 3 pixels seems to be a little bit more smooth than the 1 pixel mean, while the 100 is certainly more smooth, however this comes with a cost, as the OD is much smaller, it might still be able to give us the answers we seek, as it can clearly be seen that there are still two functions at play. On the other hand, the OD is taken over so many pixels that it is no longer just a BEC we are looking at, as some pixels which contains only thermal atoms are meaned over now, which is not ideal.

When the data points are prepared a fit is made in both the x and y direction individually to the function,

$$f_{1D}(x) = A_{\mathrm{BEC}}\cdot\max\left[0, \left(1 - \left(\frac{x - x_c}{r_{x,\mathrm{BEC}}}\right)^2\right)\right]^{3/2} + A_t\cdot\exp\left(-\frac{(x - x_c)^2}{2(C + r_{x,\mathrm{BEC}})^2}\right), \quad (4.9)$$

where A_{BEC} and A_t are the amplitudes of the BEC and thermal cloud respectively, and $C + r_{x,\mathrm{BEC}}$ is the width of the thermal cloud. This is done in the form of $C + r_{x,\mathrm{BEC}}$ in order to restrain the width of the thermal cloud to be larger than the width of the BEC. Same equation also holds for the y-direction and the same is done there. The only parameters needed for the further evaluation are the center and the BEC radius, as these two allows the program to make a mask for the BEC and thus a BEC RoI is made.

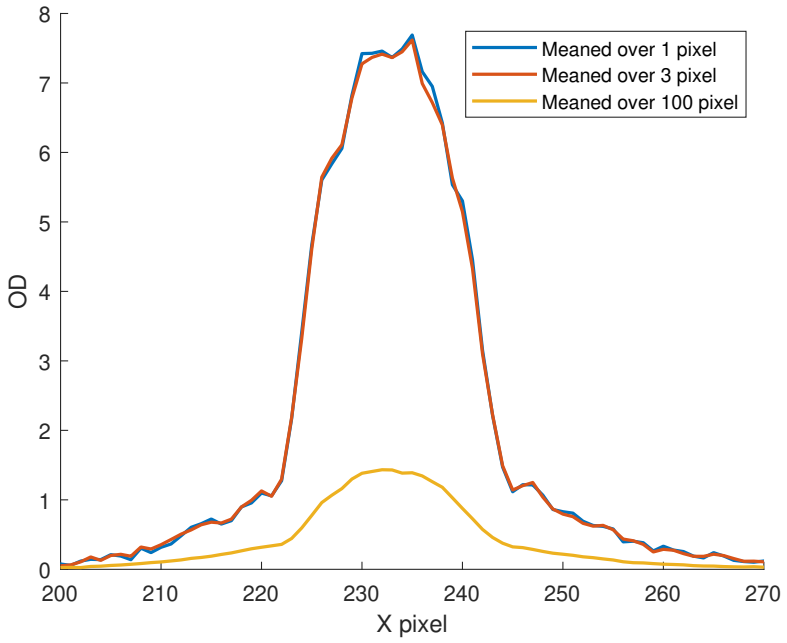

Figure 4.3: Three slices of the x axis at $y = y_c$, with the mean value taken over 1, 3 and a 100 pixels.

With a BEC RoI available a RoI for the thermal cloud is straight forward. The program takes the original defined Cloud RoI and takes all pixels that are not used in the BEC RoI and puts them in the thermal RoI.

4.3 OD calculation

With the regions of interest found we can correct for another experimental source of error. If somehow the laser or the background light changes in between the atom and beam image, this can result in a wrong OD for the image. We therefore wish to find the general ratio between the incoming intensity in the two images.

This ratio we can of course not gain from the atomic cloud, as the difference between the two images are exactly what we are looking for. Usually the atomic cloud fills only a small fraction of the total picture, the rest are just "empty" pixels. However these pixels does very rarely have OD = 0 and are a perfect way to find the offset between the two images. This is where we use the reference RoI defined earlier and it is therefore we require that there is no atoms in this RoI, as this would give a wrong ratio. This ratio is found as,

$$\text{ratio} = \frac{\text{mean}(I_{atom}(x, y \in \text{RoI}_{\text{reference}}))}{\text{mean}(I_{beam}(x, y \in \text{RoI}_{\text{reference}}))}, \tag{4.10}$$

SkyFit is now ready to define an optical depth, using a modified version Eq.

(2.76),

$$\mathrm{OD}(x,y) = \alpha \ln\left(\frac{I_0(x,y)\cdot \mathrm{ratio}}{I(x,y)}\right) + \frac{I_0(x,y)\cdot \mathrm{ratio} - I(x,y)}{I_s}, \tag{4.11}$$

where

$$\alpha = \alpha^*\left(1 + \left(\frac{2\Delta}{\Gamma}\right)^2\right), \tag{4.12}$$

where α^* is the one defined in Eq. (2.76). Eq. (4.12) is due to us not having defined a detuning in our evaluation method and due to the requirements of α, the detuning can still be included. α is known number from a previous calibration. Note that this is the expression for only the old α^*, calculated with the method shown in [15], as we have not yet implemented a spatial α calibration nor a β calibration for that matter.

4.4 Fitting routines

There are a number of different fits that can be done in SkyFit, which can be chosen in the "Model" radio button group in the middle of the left column on Fig. 4.1. The choice of button tells SkyFit which kind of fitting routine to do, whether it should do a Gaussian fit, a Bose-enhanced or a BEC fit and in what combination.

By choosing "Thermal", SkyFit only does a Gaussian fit. By selecting "BE Thermal", only a Bose-enhanced Gaussian fit is made. If "Bimodal" is chosen, both a Bose-enhanced Gaussian and a BEC fit is made, And for "Pure BEC" only a BEC fit is made. The last two options, "None" and "Cold bimodal", are extra features and will therefore be covered in Section 4.6.

This section explains the sequence of how SkyFit's fitting routines. Each time a fit is made and checks with what fitting model is used, to discern whether the present fit are to be made or not.

In the event that there are both thermal and BEC atoms in the cloud, SkyFit have to separate the two, this can become problematic as there are often both thermal and BEC atoms in the pixels. Therefore it is necessary to get a number on how many thermal atoms are overlapping with the BEC. This is done by first doing the thermal fit in the thermal RoI, where there are no BEC atoms.

The way the thermal fit is done, is by making a fit to either a Bose-enhanced Gaussian ("BE Thermal" and "Bimodal" buttons) or a normal Gaussian ("Thermal" button). This depends on the temperature of the cloud, if we are close to the critical temperature or below it, a Bose-enhanced describes the atoms best. The Bose-enhanced is based on Eq. (2.80), but modified in order to correct between our

experimental images and the theoretical prediction,

$$f_{\text{thermal}}(x,y) = f_{BE}(x,y) = \frac{C_{\text{thermal}}}{2\pi w_x w_y \zeta(3)} g_2 \left[\exp\left(-\frac{(x-x_c)^2}{2w_x^2} - \frac{(y-y_c)^2}{2w_y^2} \right) \right] + c, \tag{4.13}$$

while the normal Gaussian fit that will be done if "Thermal" is chosen, is based on Eq. (2.81) and again modified here,

$$f_{\text{thermal}}(x,y) = f_{\text{Gauss}}(x,y) = \frac{C_{\text{thermal}}}{2\pi w_x w_y} \exp\left(-\frac{(x-x_c)^2}{2w_x^2} - \frac{(y-y_c)^2}{2w_y^2} \right) + c. \tag{4.14}$$

Both fits are made through a non-linear regression model. Where c is a constant offset. c should be zero due to the ratio we found in Eq. (4.10). However this seems not to be true in all pictures. Whether to have c be in the evaluation or not, can be chosen in the GUI with the check box "Thermal fit offset". lastly C_{thermal} is an amplitude that relate closely to the atom number, but as our data are measured in optical depths and on a pixel, we have to translate it to an atom number by taking the cross section and area of a pixel into account,

$$N_{\text{thermal}} = C_{\text{thermal}} \frac{A_p}{\sigma_0}, \tag{4.15}$$

where A_p is the area of a pixel.

Note that by using the option "Center Boundness", a user decides whether x_c and y_c are fitting parameters by choosing "Fitted" or if they are defined earlier through the BEC RoI calculations, by choosing "Bound". This option is available as in the event of few atoms, the evaluation might find the center of the thermal cloud a few tens of pixels away from the center of the BEC. Fits that gives that kind of result should be wrong, as both the BEC and the thermal cloud, feel the same potential and therefore should also feel the same minimum. It is therefore a physical relevant assumption to make. However the center calculated earlier is of course not infinitely precise and the 2D fitting routines should give a better result, so if possible, "Fitted" is the better option.

The BEC fit is done pretty much the same way, but with the thermal contribution subtracted from the raw data for all pixels inside the BEC RoI. The function fitted to is Eq. (2.82), reproduced here;

$$\begin{aligned} f_{\text{BEC}}(x,y) &= \text{OD}(x,y) - f_{BE}(x,y) \\ &= \frac{5C_{\text{BEC}}}{2\pi R_x R_y} \max\left[1 - \left(\frac{x-x_c}{R_x^2}\right)^2 - \left(\frac{y-y_c}{R_y^2}\right)^2, 0 \right]^{3/2}, \end{aligned} \tag{4.16}$$

note that it is the Bose-Enhanced thermal fit that is subtracted, as at temperatures $T < T_C$, this function describes the thermal atoms seen in the image best.

4.5 Evaluation results

SkyFit gives some notably results after an evaluation. Firstly it counts how many atoms are inside the Cloud RoI, the optical density is converted to an atom number by

$$N_{\text{sum}} = \sum_{x,y \in \text{RoI}_{\text{cloud}}} (\text{OD}(x,y) - c)\frac{A_p}{\sigma_0}. \tag{4.17}$$

This sum is the only number which can be found without any fitting routines, in the event of no systematic offset in the pictures. That this number does not depend on any fitting methods, makes it a good number for a lot of applications. One just have to bear in mind that it depends on the cloud RoI.

With the fits done in Eqs. (4.13)-(4.16), the easiest result to extract is the amount of both thermal and BEC atoms, as these are just,

$$N_{\text{thermal}} = C_{\text{thermal}}\frac{A_p}{\sigma_0}\ ,\ N_{\text{BEC}} = C_{\text{BEC}}\frac{A_p}{\sigma_0}. \tag{4.18}$$

Another way to find the amount of BEC atoms is also to take sum of the OD inside the BEC RoI and subtract the thermal contribution,

$$N_{\text{BECSum}} = \left[\text{OD}(x, y \in \text{RoI}_{\text{BEC}}) - f_{BE}(x, y \in \text{RoI}_{\text{BEC}})\right]\frac{A_p}{\sigma}, \tag{4.19}$$

this number is a good sanity check when compared with N_{BEC}, as these two should give roughly the same number, but done through two different methods.

With all different kinds of atom numbers accounted for, the next interesting thing is the temperature. The temperature is calculated in both directions as;

$$T_x = w_x^2 A_p \frac{m}{k_b(1/\omega_x^2 + t_{\text{ToF}}^2)}\ ,\ T_y = w_y^2 A_p \frac{m}{k_b(1/\omega_y^2 + t_{\text{ToF}}^2)} \tag{4.20}$$

where m is the mass of the atomic species used, ω_i is the trap frequency in the given direction, t_{ToF} is the time-of-flight and w_i is the thermal width in the given direction.

This means that even for a cloud below the critical temperature, we need a thermal cloud in order to measure the temperature, making a pure BEC fit unable to give a temperature. The temperature in both directions should in theory be the same value, however they seem to differ a bit, but again this can be used as a sanity check if they are too far apart.

The temperature in kelvin is not always the best to get an idea of how cold the atomic cloud is, therefore skyFit also calculates the critical temperature and gives the temperature in terms of the critical temperature, given as

$$T_c = \hbar(\omega_x\omega_y\omega_z)^{1/3}\frac{N_{\text{sum}}}{k_b\zeta(3)^{1/3}}. \tag{4.21}$$

SkyFit also gives the position of the center and the width of both the BEC and thermal cloud, which comes directly from the fits in Eqs. (4.13)-(4.16), and are therefore in the unit of pixels. Knowing the pixel sizes makes it easy to convert it to a real length scale, however I find it more intuitive to have the numbers that are seen in the on the image.

For the optimisation mentioned in subsection 3.3.2 we found it useful to also calculate the phase space density which is calculated in both the x- and y-direction as the temperature in these directions might differ,

$$n\lambda_{dB,i}^3 = \frac{N_{thermal}\hbar^3\omega_x\omega_y\omega_z}{(k_bT_i)^2}. \tag{4.22}$$

The next result SkyFit delivers the intensity, which is found by,

$$I = \text{mean}[I_0(x, y \in \text{RoI}_{\text{cloud}})], \tag{4.23}$$

and is therefore the mean intensity in the part of the image that contains atoms, in the event of a non-uniform beam this means that the cloud RoI could have a great influence on this number.

For the work done in Chapter 5 it was important to see how many photons and how many absorbed photons there were in the image. The amount of photons in the image is found as,

$$N_\gamma = \frac{C_{\text{cam}}A_p}{E_\gamma} \sum_{x,y\in\text{RoI}_{\text{cloud}}} S_{beam}(x, y), \tag{4.24}$$

and

$$N_{\gamma,\text{abs}} = \frac{C_{\text{cam}}A_p}{E_\gamma} \sum_{x,y\in\text{RoI}_{\text{cloud}}} (\text{ratio} \cdot S_{\text{beam}}(x, y) - S_{\text{atom}}(x, y)), \tag{4.25}$$

where $E_\gamma = 2\pi\hbar c/\lambda$ and is the energy of a photon. Lastly SkyFit gives out the sum of squared errors of prediction (SSE) for both fits done.

4.6 Extra features

By now a "standard" run have been explained, however there are still a few other features that can be used in an evaluation. Of these extra feature a handful hold relevance to the physics in play and I will cover these here.

It can be useful to set the RoI check box off. This would define the cloud RoI as the whole image and therefore we would have no reference RoI. This means we can't find the ratio between the atom and beam image as described in Eq. (4.10), therefore we skip this step when calculating the OD. This is useful for very large

clouds, where defining a reference would either contain atoms or are so small that it would not be possible to give a good statistical measure for the ratio.

In Sec. 4.4 I covered four of the six buttons in the "Model" radio button group, shown in Figure 4.1. The first one skipped is "None", which is just an evaluation done without any fits. This will still give the sum, as it can be taken independently of any fits. Note, that this means the sum is calculated with $c = 0$.

If "Cold bimodal" is chosen, the BEC RoI is found by only fitting a BEC fit, meaning the second term in Eq. (4.9) is omitted. However for the 2D fits done in Sec. 4.4, this is the completely same fitting methods as "Bimodal". By choosing this option, a very cold cloud might be easier to evaluate correctly, as a low thermal signal might confuse the fit and make the RoI too big. This will then lead to the few pixels that only contain thermal atoms, becomes even fewer and a proper thermal fit might not be possible. An example of this can be seen on Fig. 4.4, where it can be seen that for low temperatures ($T/T_c \lesssim 0.75$), the "Cold Bimodal" data point seems to be more consistent, while for $T/T_c > 0.8$, "Cold bimodal" seems to be less consistent. This clearly indicates that this new feature can indeed improve our precision for low temperatures. However one thing that can also be seen on Fig. 4.4, is that the "Cold Bimodal" measurements is seen to generally have higher temperatures, which could be due to generally creating larger BEC RoIs and somehow makes the constant offset, c, larger, which in turn would lower N_{sum}

The method for finding the BEC RoI is built on the assumption that the symmetry axes of the elliptic cloud are aligned along the x- and y- axis in the image. However this is not always the case of all laboratories. If this is the case, SkyFit have a built-in image rotation, that rotates the image, a user defined number of degrees.

There are a few more features, but none of them hold any real significance in regard to the physics.

4.7 Correct usage of SkyFit

The program is made with a lot of different possibilities for evaluation. They idea is that depending on what kind of picture is used, different evaluations might be needed. If the picture that wish to be evaluated is for instance cold then the "Bimodal" method might have produce a bad BEC RoI and on the other hand if the temperature is close to the critical temperature, "Cold bimodal" might also produce a bad BEC RoI.

Under use of the program it was also found that for pictures taken in the Mixture

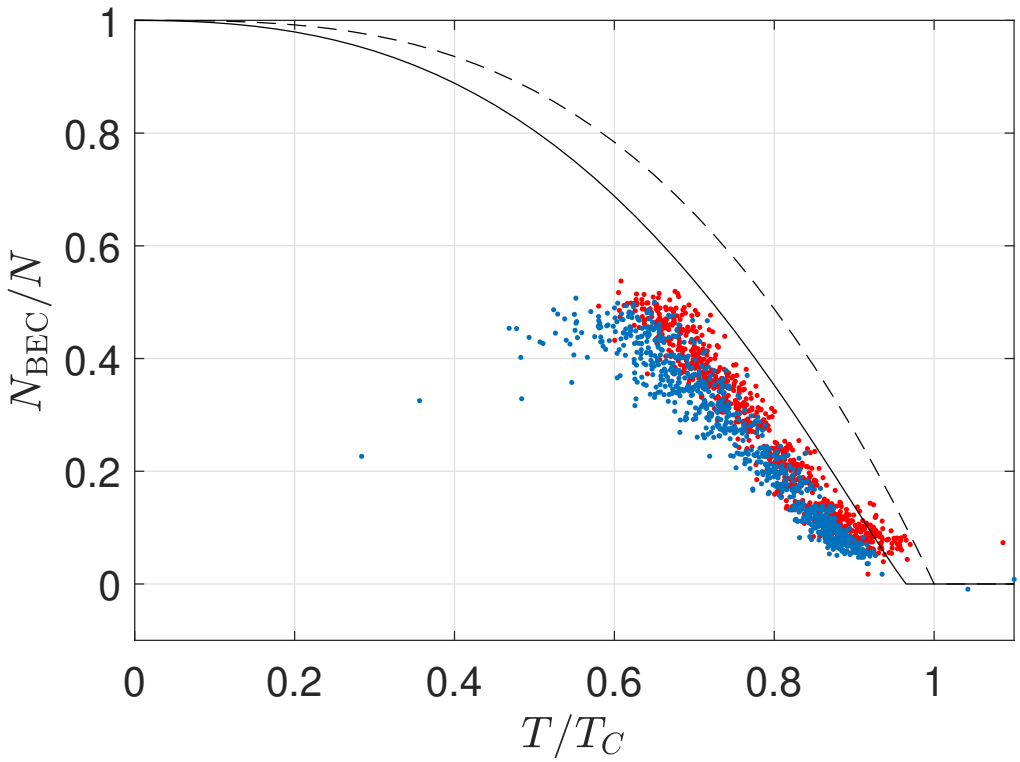

Figure 4.4: Comparison between the "Bimodal" fit option (•) and the "Cold bimodal" fit option (•) for T definitely below T_c. The same data have been evaluated for both methods, under the same conditions, except the BEC roi method. (- - -) shows the condensate fraction (Eq. (2.10)) without interactions and (——) shows the condensate fraction with the correction due to interactions (Eq. (2.28)).

laboratory, a large RoI can lead to a significant offset and calculating without the offset might lead to a temperature too high. We have observed evaluations with temperatures a good amount over T_C but still clearly with BEC atoms, thus the evaluation must be wrong. On the other hand if a fit offset is used for cold ensembles, this might give the function too much freedom, and fits almost all thermal atoms to be a fit offset and thus getting a clearly wrong estimate of the temperature.

These are examples of situations where SkyFit is able to actually do the job even better than using the old method where there is no fit offset nor an option like "Cold bimodal", but it might as well do it worse. SkyFit is therefore a tool with the possibilities to go even further than before, but only if the user takes care to choose the settings that best describes the situation. However it is still possible to make it easy for the user and just do the old method, if this is to be desired.

4.8 Evaluation of SkyFit

At its current state, SkyFit is able to do the required evaluations and to the best of my knowledge all three laboratories are at least trying to out-phase Perfectfit. With program being Git-controlled, some measure of streamlining should be achievable, so that all three laboratories are using the exact same program.

SkyFit should also be somewhat editable as of yet. Put all of this does not really matter if the evaluations are wrong, or at least not as wrong as evaluations of the same images, but with the old program.

It is not an easy thing to test whether we have improved the accuracy compared to Perfectfit, but we can look at the condensate fraction as it is described in Eqs. (2.10) and (2.28), but one must bear in mind that these are both approximate expressions and therefore our measurements should not necessary coincide, but the general trend should be somewhat the same. This can be seen on Figure 4.5. First and foremost it should be said that Perfectfit does not make a Bose-Enhanced thermal fit as seen in Eq. (4.13), but instead fits the thermal atoms to a Gaussian 1D fit as seen in Eq. (4.8). This would give another width, but it could also mean that the difference between the more peaked Bose-Enhanced fit and the pure Gaussian would wrongly be fitted as a BEC.

With the comparison seen in Fig. 4.5, SkyFit seems to have a few advantages over Perfectfit. Firstly it seems to be able to get more correct temperature. It is also clearly better to distinguish small BECs, as the SkyFit points shows a systematic start around the same point as the full black line have start having$N_{\mathrm{BEC}}/N \neq 0$. If one ignores the weird outliers, it also seems like SkyFit is a bit more precise, if not by much, especially at low temperatures, where Perfectfit seems to almost explode.

On two points does SkyFit seem to fail, firstly some fractions are negative, which is of course impossible and extremely high fractions around $T/T_c = 1$. Both are due to SkyFit evaluated the images with its "Bimodal" setting, through all these runs, which means it will always fit to a BEC and if there are no BEC, then this will be problematic and can give wrong fits. In the case of negative fractions, this is however not a purely negative thing as it clearly shows a user that the "Thermal" or "BE Thermal" fit-option was the better solution. This could be remedied by putting a lower bounds on the BEC fit, but as the thermal fit is done first, a negative BEC means this one failed, which would be done to a wrongly estimated BEC RoI, so removing the BEC RoI would give the most correct answer, so by not having a lower bound for the fit, it is a lot easier to sort these wrong evaluations away.

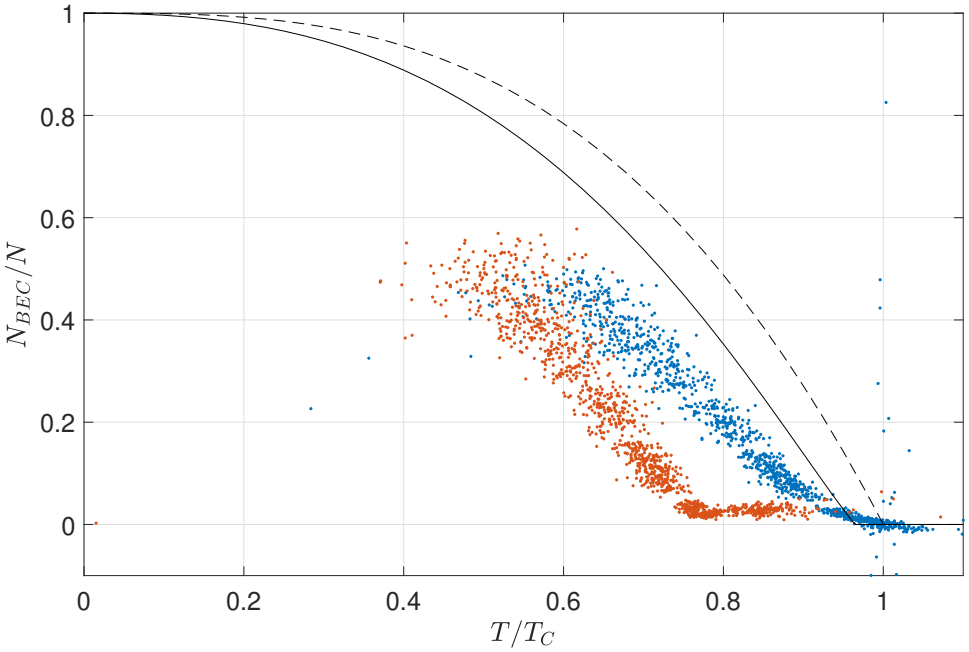

Figure 4.5: Comparison between SkyFit doing a "Bimodal" fit (•) and Perfectfit (•) evaluations. No sorting in the data have been used and all SkyFit evaluations are done under the same conditions, the same is true for Perfectfit evaluations. The summed atom number from the two programs are close to each other. (- - -) shows the condensate fraction (Eq. (2.10)) without interactions and (——) shows the condensate fraction with the correction due to interactions (Eq. (2.28)).

Chapter 5

Spatial α Calibration

5.1 Introduction

This chapter describes the work done in our investigation of the spatial dependence of the calibration parameter, α^*. This is still a work in progress, and we are currently drafting an article. The work here was done in close collaboration with Mick A. Kristensen and Mikkel B. Christensen, where my primary contribution was taking the data.

5.2 Old calibration method

As it was described in Sec. 2.3, there are a few corrections to the ideal imaging system. The α correction outlined in [15], which can be seen in Eq. (2.76), states an correction to the imaging saturation in order to take impure light polarisation and Zeeman sub-level populations into account. A method to correct for this is shown in [15], which is the article we based our old calibration method on. The method described here, utilises the fact that the atomic density does not depend on the intensity of the incoming light. In practice this is done by simply varying the intensity and then try for different α^* values, in order to see which α^* gives constant optical density, when using Eq. (2.76), where the optical density is extracted from the point containing the highest OD. This method uses a constant incident photon numbers, which is held constant by changing the duration of the laser pulse, as the intensity is changed. An example of a calibration is seen in Figure 5.1, where the black line shows the best line.

In [15] this is done for low absorbed photon numbers per atom ($N_{\gamma,a}/N \sim 5$), as absorption of a photon might lead to pushing and heating of the cloud, which

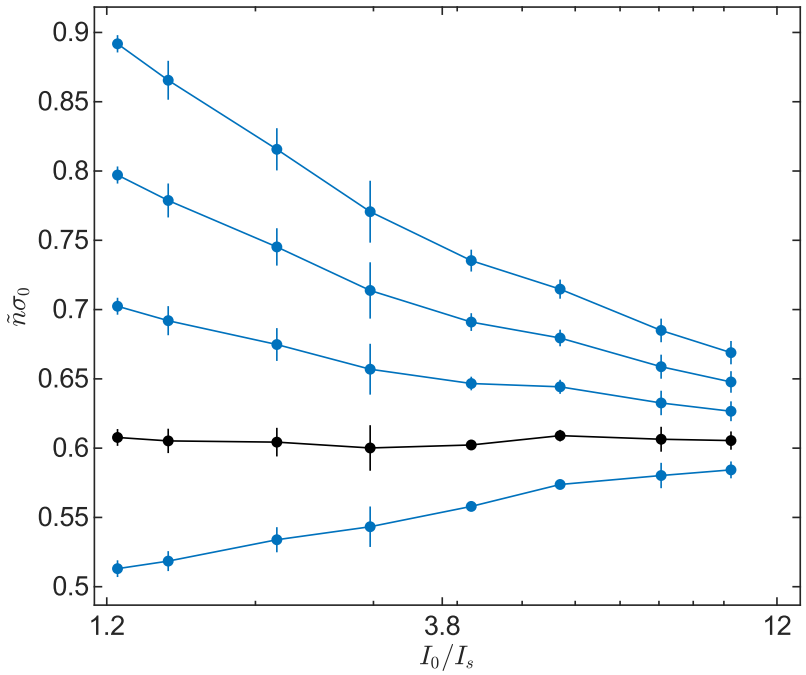

Figure 5.1: Using the method described in [15], images are taken at different intensities of the laser beam (I_0) and 5 different α^* values are chosen to see what they give. The black line show the best behaviour and the α^*-value corresponding to this, is the best one.

might lead to changes in the imaging conditions, which will be presented in the next section. This is also why the incident photon number is held constant, in order to suppress the amount of absorbed photons.

5.3 Photon effects

In our experiments we try to have as precise measurements as possible and this requires a high signal-to-noise ratio, which means we usually do not have only 5 photons absorbed per atom, but a lot more.

Absorption will lead to heating, pushing and other more complicated effects. As the number of absorbed photons per atoms does not follow the amount of incident photons in case of saturation effects, this means, if we keep our incident photon number constant, by finding the right combination of intensity and detection time, the absorbed photon number will change throughout a dataset. How great of an influence this causes can be calculated to some extent by doing a back-of-the-envelope calculation for the Doppler detuning, Δ_D, each absorbed photon makes. For our absorption images we use the D2 line in ^{87}Rb and we can assume our laser frequency

is at the natural frequencies of our atoms, giving,

$$\begin{aligned}\Delta_D &= \omega_0' - \omega_L = \omega_0 - \omega_L + \frac{\omega_0 \Delta v}{c} = \frac{\omega_0 \Delta v}{c} = \frac{2\pi \Delta p}{m\lambda} = \frac{2\pi p_\gamma}{m\lambda} \\ &= \frac{(2\pi)^2 \hbar}{m\lambda^2} = 2\pi \times 7.536\text{kHz},\end{aligned} \tag{5.1}$$

where Δv, Δp are the change in velocity and momentum of the atom, m mass of the atom and p_γ is the momentum of a photon. From [21], the natural linewidth is $\Gamma = 2\pi \times 6.065(9)$MHz. For our experiment we wish a high signal-to-noise ratio, which means we generally require $N_{\gamma,a}/N \gtrsim 100$, we can therefore calculate the Doppler shift for 100 $N_{\gamma,a}/N$,

$$4\left(\frac{100\Delta_D}{\Gamma}\right)^2 = 6.2\%, \tag{5.2}$$

indicating that for $N_{\gamma,a} \geq 100$, the Doppler shift plays a significant role. The method discussed in the previous section seems to be good enough for low absorbed photon numbers per atom, however for experiments with $N_{\gamma,a}/N$ on the order of 100 this is no longer expected to be the case.

It is therefore possible that the direct method described in [15], is not viable for our case. Therefore our idea is to still use the general method outlined in [15], after all, the requirement that the intensity does not change the atom number must hold. But our first idea is to use a constant $N_{\gamma,a}/N$ instead, thus having the same effect from absorption in all images. This is however not as easy to accomplish as constant incident photon numbers, mostly because it does not scale linearly with pulse duration or intensity, due to saturation effects.

But before we do any measurements, lets look at the limitations we have when doing a calibration. The intensity is in principle limited by both the available incoming beam intensity and the saturation of the camera. In reality the camera sets the limitations on the intensity, as it saturates at intensities lower than the physical range of intensities at our disposal. A loose requirement is also that the intensity must be large enough to shine through dense clouds, but we do not want it so large that all atoms are saturated. This makes it favourable to use thermal atoms, instead of BEC atoms. In regard to the resolution we can achieve, when the comes to control of the intensity, we have inserted a half-wave plate and a polarising beam cube in the imaging path and are therefore able to fine-tune the intensity to a reasonable resolution. There are still small changes in the intensity, but they are on the order of 1% from run to run.

The other available control parameter we can change to see the wished number of incident and absorbed photons is the pulse duration. The upper limit of the pulse

time are imposed by the effects of the cloud during time of flight, we do not wish the pulse to be so long that the atoms have time to fall significantly during imaging, we take our images after 12 ms of time of flight, and we can calculate that for $t < 32\,\mu s$, the cloud moves less than one vertical pixel. The lower bound is set by our set-up, where a acoustic optical modulator that we use to or imaging beam on and off, is able to give square pulses for $t < 1\mu s$. As was seen in Sec. 2.2, a crucial assumption for the absorption imaging is to be in the steady-state, this can be assumed to hold for $t \gg 1/\Gamma = 165\,ns$. In regard to the resolution of the pulse length, it is set digitally in units of 1µs, this would limit our control of the pulse duration significantly, so we decided to circumvent this by using an external signal generator, making it possible to produce imaging pulses with control of the time length on the order of ns. This makes us able to have a precise control of incident photon number and thus also the absorbed photon number.

Given that we are using atom number stabilisation, we are also able to keep the atom number constant, then by doing a qualified guess on what intensities and pulse duration give a given $N_{\gamma,a}/N$ and then iterate until we are at a wished $N_{\gamma,a}/N$, we are able to do a calibration, based on constant $N_{\gamma,a}/N$, instead of constant incident photons.

With a theoretical prediction and the technical capabilities record clouds over large spans of incident intensities, while keeping the number of absorbed photons constant, we can try to test how constant incident photon numbers compare to constant absorbed photons per atom. This can be done by doing the α calibration as outlined in the previous section, for a few different constant photon numbers and then a few different constant absorbed photon numbers. This is done with all clouds of equal stabilised atom number and at low densities, for reasons that will be apparent in the next Section. The result of this can be seen on Fig. 5.2, where we see how an α-calibration depends on both the incident photon number and the absorbed photons per atom number.

The analysis of Fig. 5.2 gives a clear indication that for high incident photon numbers, α depends on the amount of incident photons, while the dependence seems a lot less outspoken if we calibrate after constant absorbed photons per atom.

This shows quite good agreement with our initial guess based on Eq. (5.2), while also being in agreement with [15], as this article works in the regime of low incident photon numbers, where they seem to have about the same α. But for higher incident photons, it gives a completely different α value. Whereas the absorbed photon number per atoms, seems a lot more constant. However it is still not perfect and it

shows there still might be effects unaccounted for, but for now, this figure gives a clear indication, that absorbed photons per atoms gives a more general estimate of α, even if not a perfect new estimate.

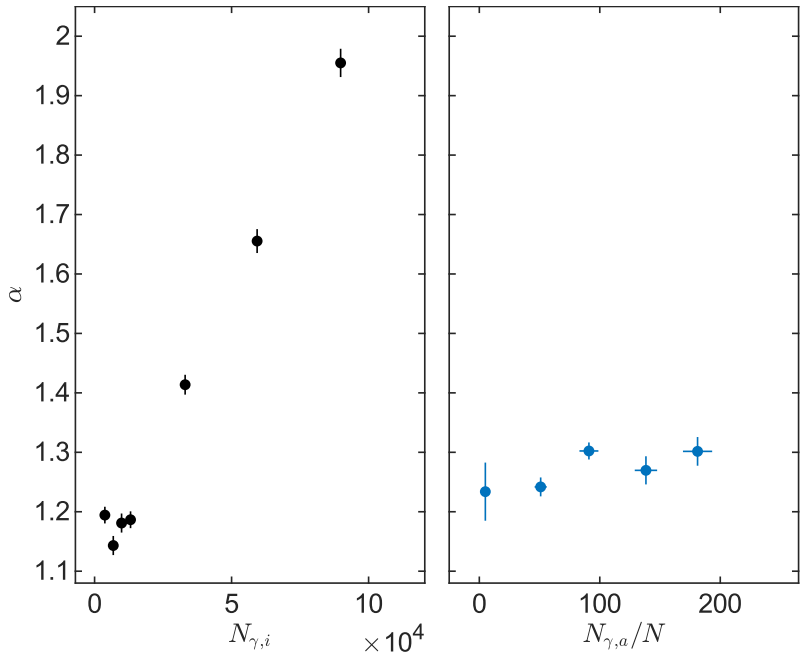

Figure 5.2: Comparison between the two different calibration schemes. For all measurements, the method shown in Fig. 5.1 are used. On the left side I_0 and the pulse duration are chosen, such that the amount of incident photons are constant. On the right, I_0 and the pulse duration are chosen, such that the amount of absorbed photons per atom is constant. The values of these two parts correspond somewhat, meaning the highest in both parts share one combination of pulse duration and I_0.

5.4 Spatial α calibration

As it is now shown the amount of absorbed photons per atom is a better calibration parameter at low densities, where effects from the atoms themselves are insignificant. However, as it is shown the amount of absorbed photons per atom makes a difference, the atoms density might also make a difference, for instance, the center atoms of the cloud where density is high will absorb on average less photons than the outer region due to screening and therefore receive a lower momentum kick during an imaging pulse and thus a lower Doppler shift. We therefore investigate how the α calibration might change, as the density changes. This we can do by dividing the cloud into a number of different rings, where each ring are chosen to yield equal intervals of $\ln(I_0/I)$.

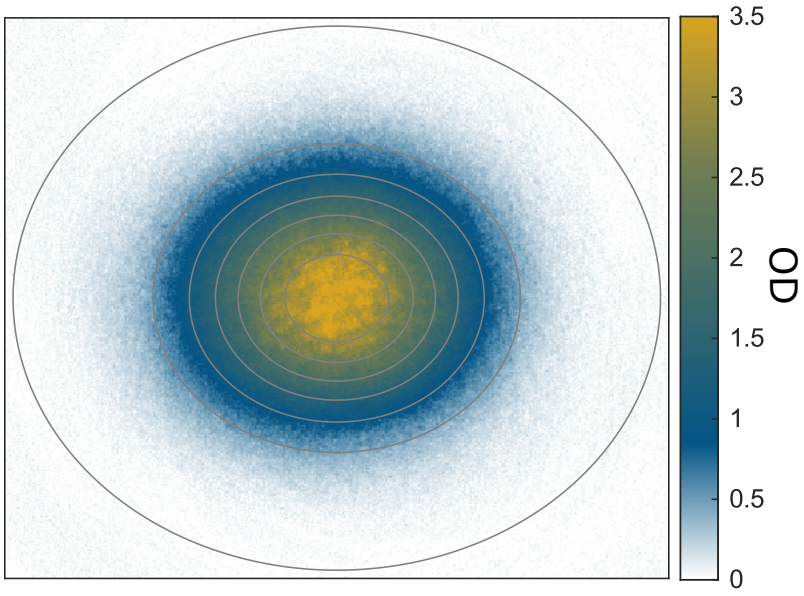

Figure 5.3: Example of how we slices up a atomic cloud for the spatial α calibration.

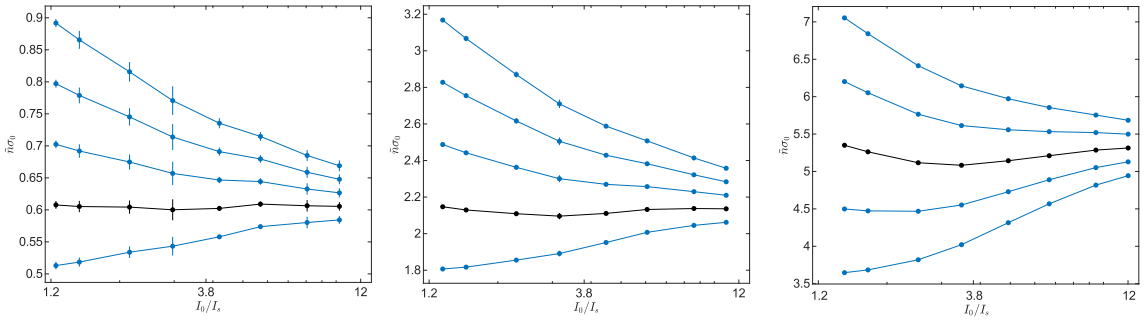

Figure 5.4: The calibration is done for different rings of the same cloud, each with different $\sigma_0\tilde{n}$. The black lines correspond to the optimal α.

As it was shown in the previous Section, the α calibration depends on the detuning, which depends on the amount of photons absorbed by each atom. This can differ spatially, if the beam is inhomogeneous. The density of the cloud also plays a role, as the atoms that the laser beam hits first might screen for the atoms further along the beam path. An atom can also decay and send a photon in a random direction that can get reabsorbed, this is ordinary not a problem, unless this leads to saturation, which would also depend on the atomic density.

We can check for these effects by looking at the different rings and see how the α calibration might look. This is done in Fig. 5.4, where the α calibration is done for three different rings, where it is easily seen that $\tilde{n}\sigma_0$ is different for the three different rings, indicating that we have a spatial dependence.

With it now established that the old α-calibration does not correct for all effects at high $N_{\gamma,a}/N$, it is therefore necessary fir an α that depends on the atomic density. This is what is tried and shown in Figure 5.5. Here it can be seen that a spatial

dependence is definitely better, than a constant α, for our measurements. Even though there are some points that seem to be a bit off. Especially the lowest one, but this is properly due to our beam being inhomogeneous and falls off about 20% in intensity from the center to the edge of the cloud. Because of the Gaussian profile of the beam and the outer ring having the highest area, these effects are more pronounced here.

By looking at the inlay, we can also see that this method is not perfect, as the fit slope changes for different constant $N_{\gamma,a}/N$. Based on Fig. 5.2, it still seems to be a better calibration, than if constant incident photon numbers were used.

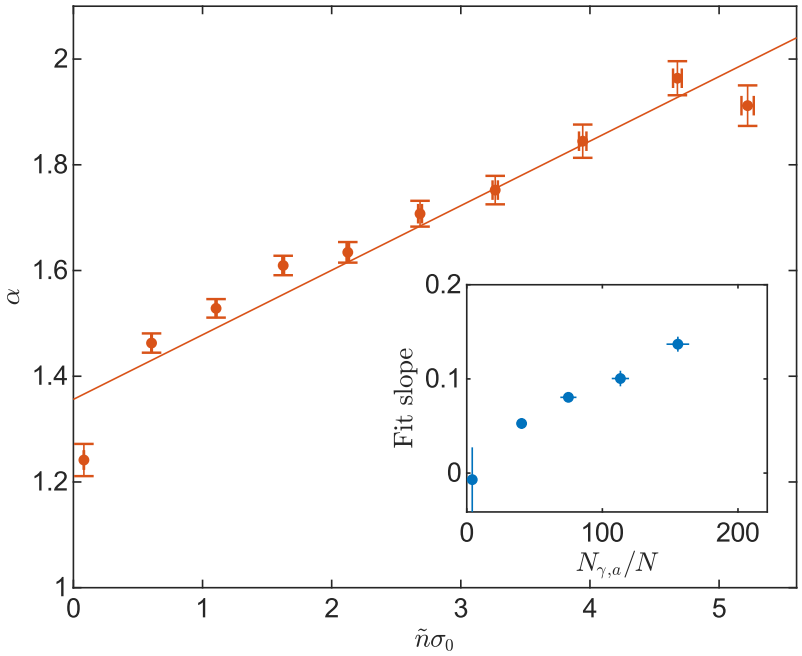

Figure 5.5: α-calibration done for different $\tilde{n}\sigma_0$, then fitted to a linear curve, in order to get an expression for α. The inlay shows how the slope of this curve looks for other constant absorbed photons per atom measurements.

By taking a look at Fig. 5.4 again, one can see that the curve seems to have a more curved structure as $\tilde{n}\sigma_0$ is higher, investigation can be expanded to include more rings, a result of this is seen on Fig. 5.6, where the whole image have been divided into ten sections, and all rings are displayed. What Fig. 5.4 illustrate is for low $\ln(I_0/I)$, a line corresponds very good to the data points, while for higher $\ln(I_0/I)$, the data point are no longer on the line. Indicating that there might be some other effects at high densities, that we do not correct for as of yet.

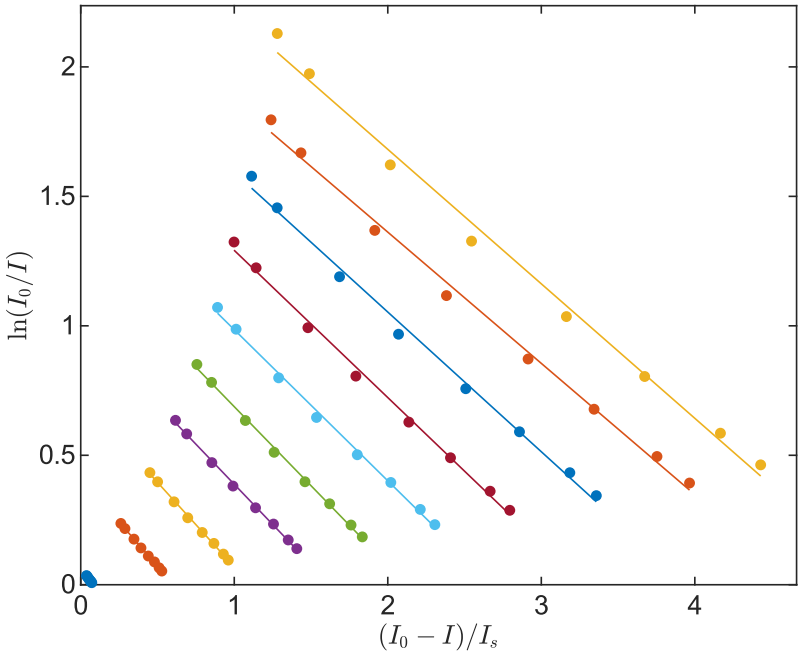

Figure 5.6: The images have been split up into 10 rings and each ring have been calibrated using the method seen on Fig. 5.1, we look at how the two terms in Eq. (2.76), correspond to each other. α correspond to the inverted line slopes. The slope and α increase for inner rings, with the inner most ring corresponding to large yellow line on this figure.

5.5 Discussion

Our investigation definitely shows that absorbed photons per atom is a better number to use than incident photon number, in the sense that it the α-coefficient varies less, as $N_{\gamma,a}/N$ is varied. This shows that the method previously outlined in [15] can not be directly transferred into higher photon number regimes.

We also present data that gives a clear indication on how the α-coefficient changes for different atomic densities. This we also show a way to correct for, where the fitted line on Fig. 5.5, clearly shows a non-zero slope, with good correspondence between data points and fits, except in the start and end.

Our new methods clearly strengthen the accuracy we are able to achieve, but this investigation also shows that there are still effects we are not correcting for and thus our calibration is not a complete answer in order to get the measured densities to be independent of the intensities, but it is a step in the right direction and can still improve our the accuracy.

Chapter 6

β calibrations

This chapter presents my work on calibrating the β parameter in the Lattice experiment. This work was mainly done in collaboration with Mick Kristensen, but of course the whole Lattice group was involved through discussions. Unfortunately this proved to be a task more complicated than first anticipated and we therefore decided there were other and more productive things to investigate in the experiment. This work was therefore not continued beyond what is presented in the present chapter.

6.1 Calibration procedure

The α constant was discussed in section 2.3 as a dimensionless constant correcting I_s not being ideally as the theory suggest. The β parameter does much of the same, except it is to correct for the scattering rate, Γ. The idea of this measurement is to correct the OD, by using that the width of the condensate, depends on the number of BEC atoms as seen in Eq. (2.41), and can be determined independent of the errors of the optical density. By comparing the measured width of the BEC with the theoretical value from (2.41), we can get a measure of the β-parameter. This is then done for different time of flight. By doing this for a few different BEC numbers, which are controlled by the final evaporation frequency and the hold time of the BEC, we should be able to get a general measure for β.

This experiment utilises our Faraday stabilisation, such that the atom number can be regarded as the same from run to run, as long as the final evaporation frequency and BEC hold time is the same. As it can be seen on Figure 6.1, this is of course not entirely true, as the atom number seems to fluctuate a bit. However in regards to atom number, all measurements below 10ms can be disregarded as the cloud is too dense to get a good estimate of the atom number. However the radial expansion

seems to quite consistent.

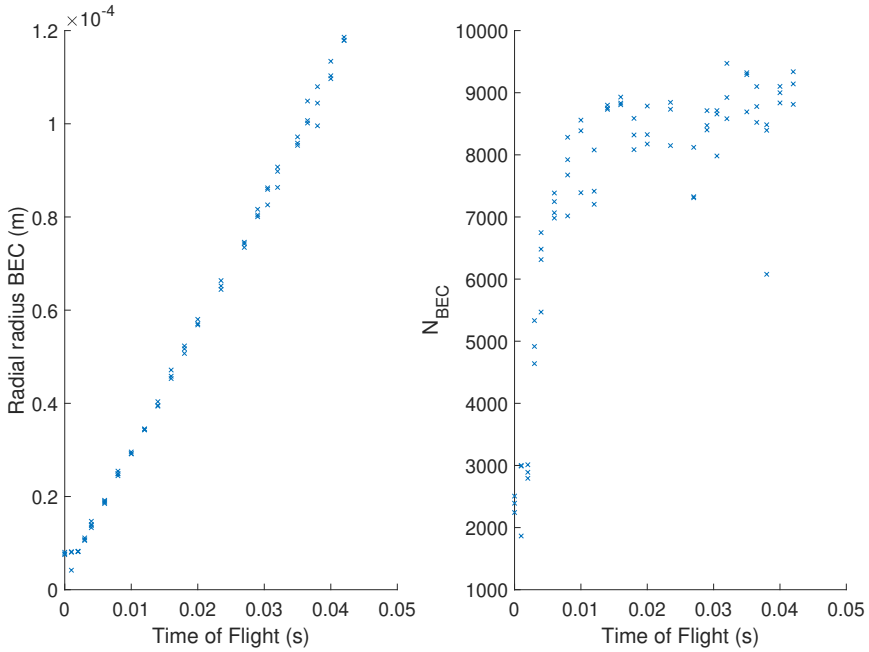

Figure 6.1: Example of a dataset with the "same atom number". Worth noting is that this is the dataset with the lowest atom number.

Figures looking like Figure 6.1 was made for 5 other mean atom numbers, ranging from $\sim 9\ 10^3$ to $\sim 1.1\ 10^5$ BEC atoms.

These results are compared to a numeric solution of equation (2.38), with the assumption that the trap turns off instantaneously. This is used in equation (2.41), but with the β value in front of the BEC number,

$$w_j = \left(\frac{15\hbar^2 a\bar{\omega}^3 \beta N_{\mathrm{BEC}}}{\omega_j}\right)^{2/5} \frac{\lambda_j}{m^{2/5}}, \tag{6.1}$$

where N_{BEC} is the mean atom number for all runs with a time of flight greater than 10 ms. By taking the data for all the different atom numbers for time of flight ranging from 0 to 42 ms and fitting to Eq. (6.1), Fig. 6.2 appears. This gives a fit of $\beta = 1.7208$, which is larger than expected. By a closer look at Fig. 6.2 two new problems presents themselves. First, for both curves, the lowest points seem to be quite off. Second in the radial direction it seems like the data points are on point or a bit above the theoretical line. However, in the axial direction, if we disregard all points lower than $t_{ToF} < 5$ ms, then the data points are systematically lower than the theoretical prediction.

This we can explain by the assumption, that the trap turns of instantaneously. This is a bad assumption as we are using a magnetic trap with 300A sent through it. First and foremost turning off that high a current takes time, in the current set-up

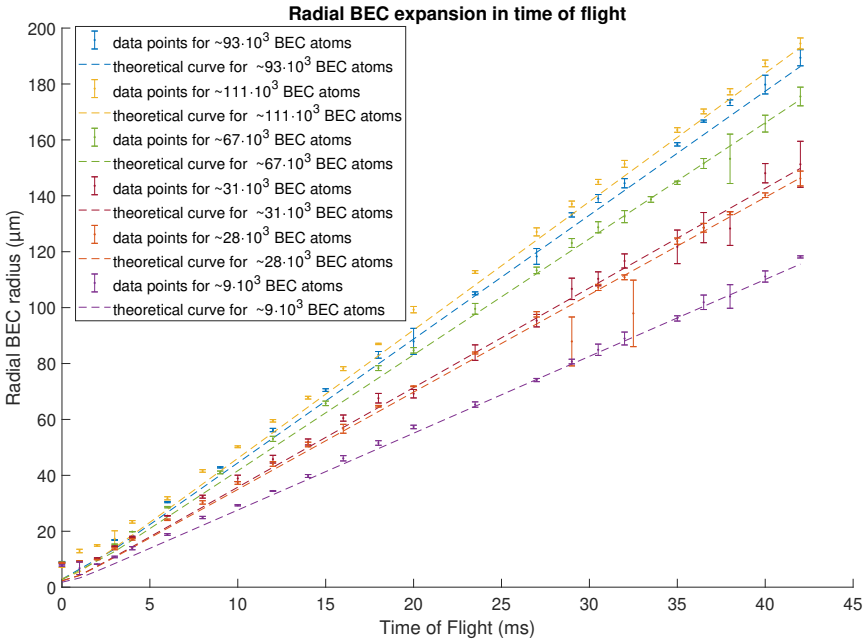

(a) Radial expansion, instant turnoff

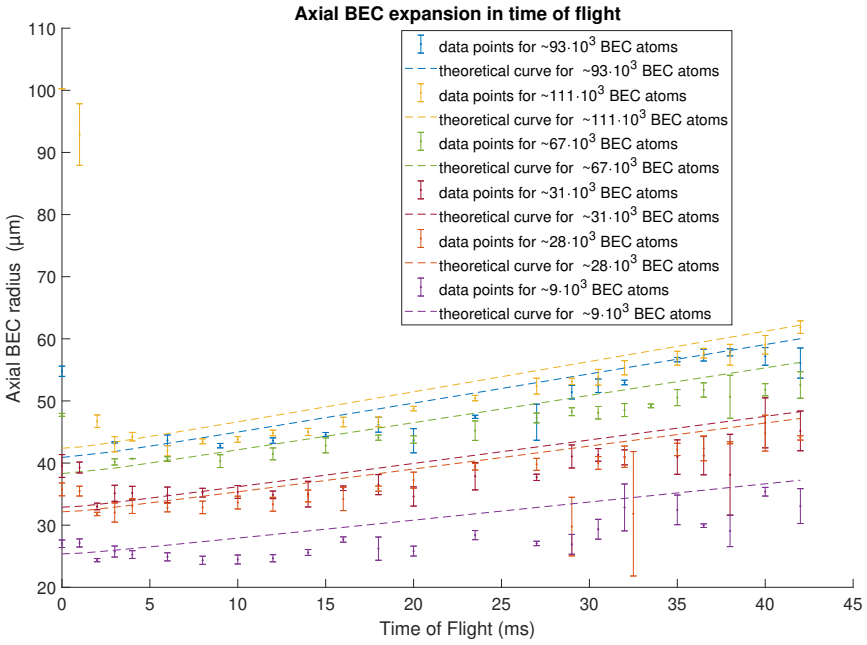

(b) Axial expansion, instant turnoff

Figure 6.2: Expansion of the BEC for the 6 different atom numbers for both the axial (a) and the radial (b) direction. The trap turn-off is regarded as instantaneous. For the BEC atom numbers stated, the mean is taken for all runs with time of flight greater than 10ms. Each point holds at least 3 different measurements. This yields $\beta = 1.7208$.

we are using an IGBT to turn off the current faster than the power supply can, but due to the inductance of the wires, it still takes about 100µs to turn it off, as can be seen on Fig. 6.3. Secondly turning off a magnetic field will also induce Eddy currents, which in turn would make the magnetic field turn off slower.

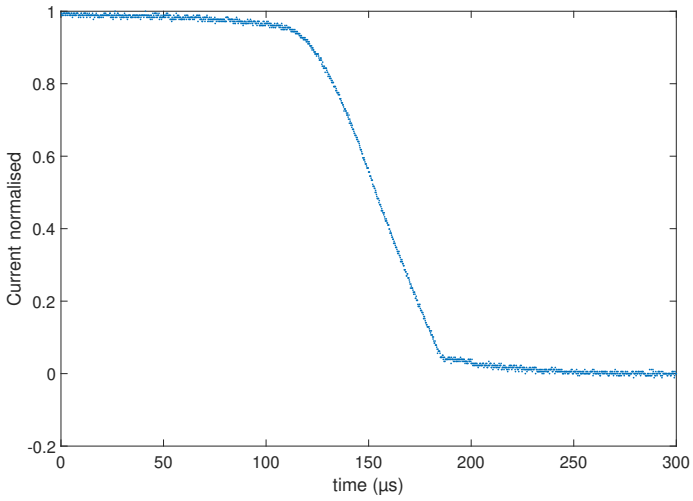

Figure 6.3: Turn off time of the current measured with a Hall-probe over a wire going to the QUIC setup. Note that this only measures the current through the wire at a certain point and with the IGBT closed, which means any Eddy currents induced are not shown here.

If we look at equation (2.42), it can be seen that it is only the trap frequencies and the expansion parameter that decides the aspect ratio. As the decay of the trap frequencies are parameters in equation (2.38), we should be able to fit for the decay of the current by fitting to the aspect ratio, under the assumption that, the current have an exponential decay, as seen in equation (3.12). The differential equation for the scaling parameter then becomes,

$$\ddot{\lambda}_j = \frac{\omega_j^2(0)}{\lambda_j \lambda_1 \lambda_2 \lambda_3} - \omega_j(0) e^{-t/\tau} \lambda_j \quad (j = 1, 2, 3). \tag{6.2}$$

This is then plotted a few decay constants in Figure 6.4, where it is seen that no matter what τ is chosen, it will only lower the curve and therefore move our simulated curve away from the data.

The reasons behind the dicrepencies between data and theory, could be due to phase fluctuations, which we observed as stribes in our images of the BECs. This could have messed up our data, so we decided to take a more spherical trap, as these are better at suppressing phase fluctuations [22].

This we can investigate by changing the background field (B_0 in Eq. (3.9)) and taking a few measurements. By increasing the z-shim current from 0.05 A to 4A,

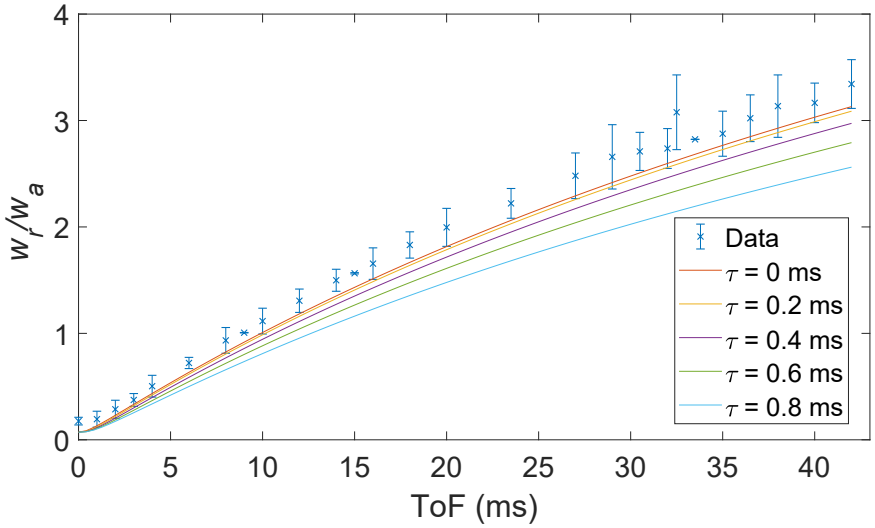

Figure 6.4: Aspect ratio simulated with different decay constants. Each data point is made from around 18 measurements.

we only lower the radial trapping frequency, which makes the trap more spherical. This gives trap frequencies of $\omega_r = 2\pi \cdot 96.670(13)\,\text{Hz}$ and $\omega_a = 2\pi \cdot 17.739(5)\,\text{Hz}$. Then we took images at 5 different high time of flight. The aspect ratio for this decompressed trap is seen on Figure 6.5, where the theory and our measurements still does not seem to correspond. This lead us to the investigate whether the two trap frequencies have the same lifetime.

6.1.1 Trap frequency decay investigation

If we take a look at equation (3.9) and use the linearity between the magnetic field and the current, we can be write the trap frequencies as,

$$\omega_\rho^2 = \frac{\mu}{M}\left(\frac{(c'I)^2}{c_0 I + B_{shimZ}} - \frac{c''I}{2}\right) \quad \text{and} \quad \omega_z^2 = \frac{\mu}{M} c''I, \tag{6.3}$$

where the c's denote the constants needed to give the corresponding B (e.g. $c_0 I = B_0$). It is then easily seen that $\omega_z \propto \sqrt{I}$, while this is not the case for the radial frequencies, as long as there is a bias field.

This lead us to investigate this further trying to simulate our trap, where the magnetic field is given by the Ioffe-Pritchard trap as seen in equation (3.4). This time B_0 includes both the bias field from the QUIC trap itself and the field from the z-shim coil.

The frequencies are given by equation (6.3), where the contribution from the z-shim coil is known by an old calibration. This means that if B_0^{QUIC} and the trap frequencies are known, then both B' and B'' can be found through the expressions

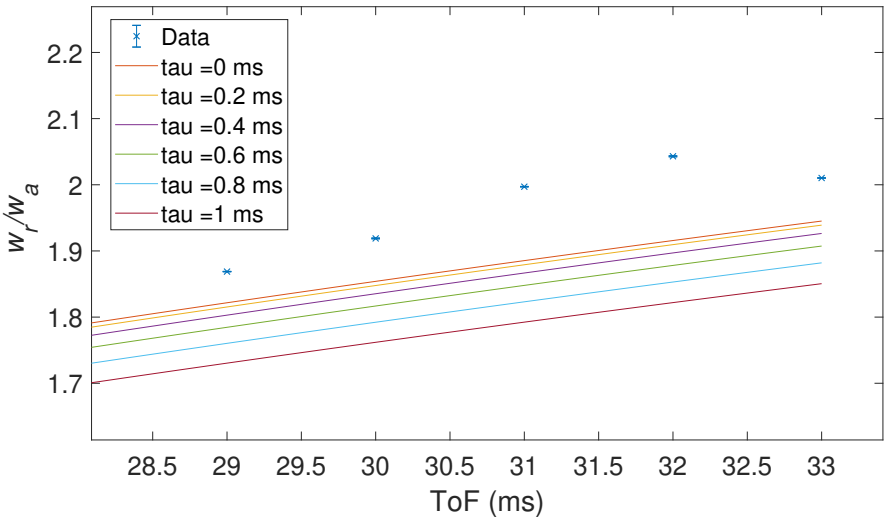

Figure 6.5: Aspect ratio simulated with different decay constants, this time for the decompressed trap, made by setting the z-shim current to 4A. It have trap frequencies of $\omega_r = 2\pi \cdot 96.670(13)$Hz and $\omega_a = 2\pi \cdot 17.739(5)$Hz. each point is made from 3 measurements.

seen in equation (6.3).

B_0 is found through the following equation,

$$B_0^{\text{QUIC}} = \frac{\hbar\omega_{\text{bottom}}}{g_f \mu_B}, \tag{6.4}$$

where ω_{bottom} is the lowest frequency that can remove atoms. This frequency corresponds to the energy of the atoms with the lowest energy, due to Zeeman splitting, which are confined at the magnetic field minimum of the trap. B' and B'' can then be found through Eq. (6.3), when the trap frequencies known.

With the field in all directions clearly defined, a few points around the center is calculated and then fitted to Hooke's law,

$$U(\mathbf{r}) = \frac{1}{2}k(\mathbf{r} - \mathbf{r}_0) + U_0, \tag{6.5}$$

where k is the spring constant and gives us the trap frequency by,

$$f_i = \frac{1}{2\pi}\sqrt{\frac{k_i}{m}} \qquad (i = x, y, z). \tag{6.6}$$

This of course only holds if the trap is an harmonic oscillator, which the trap fulfils, as seen in Figure 6.6. Here, the magnetic field is simulated for $I = 300$A and $I_{zShim} = 4$A.

Armed with a tool able to calculate both trap frequencies for all different currents, it is then possible to simulate how both trap frequencies decay. We didn't have any

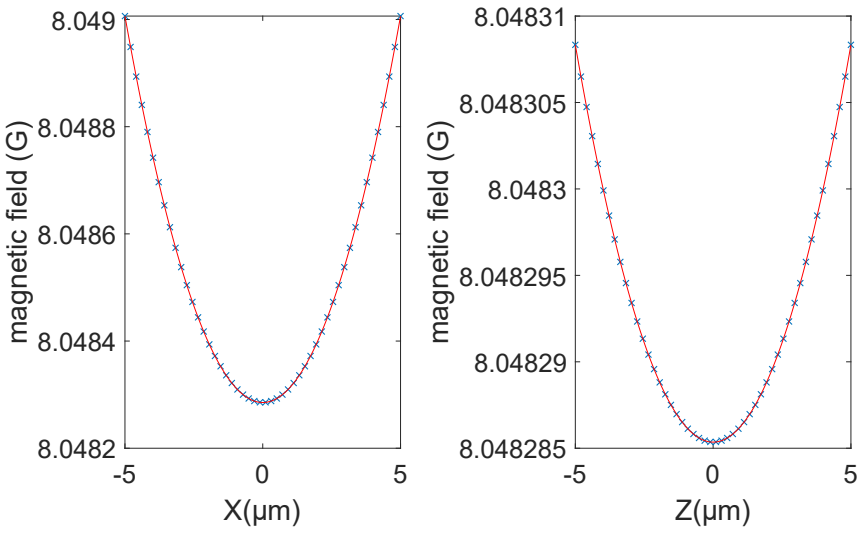

Figure 6.6: Magnetic field at $I_{QUIC} = 300$A, around the center of the trap in both the radial-direction and axial-direction.(—) shows the fitted curve to the simulated data.

theoretical expression to fit to, which lead us to fit to a general case, $\omega_i(I) = a_i I^{b_i}$. This can definitely describe the axial decay, and as seen in Fig. 6.7 it also holds very nicely for the radial part. This result shows us that the two trap frequencies definitely decay differently and that it should be possible to fit the decay as a power function.

The simulations can then be verified by experimental measurements. We measure the decay of the trap frequencies by making a BEC, then during the BEC hold time, we lower the current to the current we want to measure the trap frequencies at, here it will oscillate for at least 1 period before we turn off the trap. Then we will look at the oscillations as described in subsection 3.3.5.

We start the oscillations either by the method described in subsection 3.3.5, just before we lower the current, or the oscillations are started by the current lowering, this depends on how far the current is lowered. If the oscillations are started by lowering the current, the oscillations are started because the center of the trap moves, this gives close to no contribution for the currents of 200A or higher, but for especially for 50A this is all that is needed, with oscillations of around 40 pixels in both directions.

The result of these measurements can be seen on Figure 6.8 with decays of $b_r = 1.01(7)$ and $b_a = 0.53(6)$. The only point that is problematic here, is the point for $I = 50$A, which seems a bit off compared to the rest and this might suggest that something else is interfering with our experiment, when the confinement is weak, or

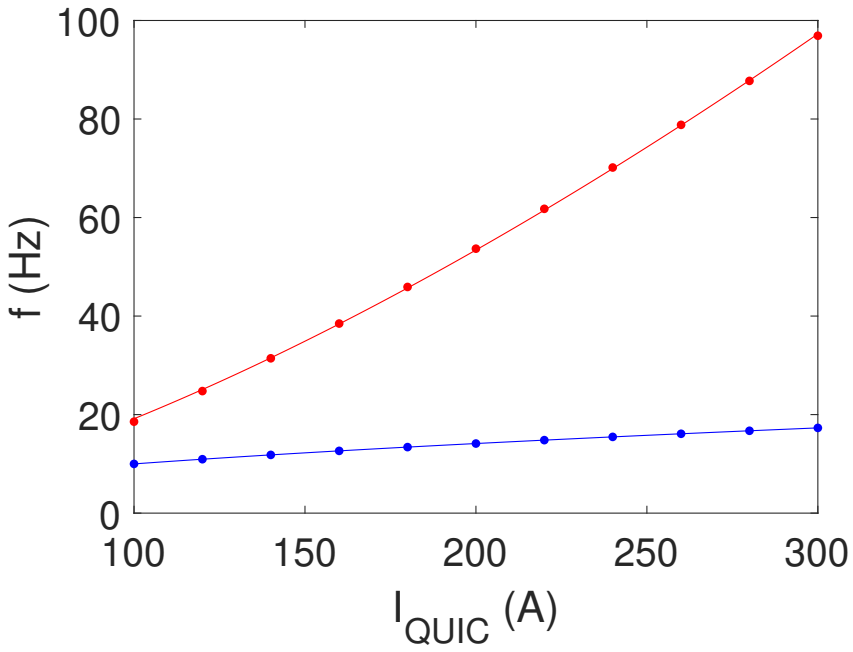

Figure 6.7: Simulation data of the trap frequency decay for $I_{zShim} = 4$A, fitted to $\omega_i(I) = a_i I^{b_i}$. Where the axial decay (•) gives $b_a = 0.050$ and the radial decay (•) gives $b_r = 1.49$.

that the QUIC trap is not described by the equations for the Ioffe Pritchard trap at low currents.

For the axial decay, all methods seems to be in agreement, the analytical, the simulations and the experimental result all say $b_a = 0.5$ is well within the uncertainty. For the radial direction the fit seems rather good, but the value is only around 2/3 of the predicted value from the simulation. This again might suggest there is something else happening we are not aware of. Worth noting is perhaps also, that neither the simulation nor these decay measurements does account for induced Eddy currents.

We then define a general lifetime τ, where $\tau_a = 0.5\tau$, and τ_r is either 1τ or 1.5τ for the decompressed trap we can try to fit both possible τ_r in order to find the decay constant. The result of this can be seen on Figure 6.9, which actually seems to fit with a relative good precision. However keep in mind this is to a incomplete dataset and the points for the same time of flight on Fig. 6.4 also seems to correspond decently with $\tau = 0$.

These data are therefore still inconclusive, especially because it seemed like if the fit is raised in one part of the fit, then it is lowered at the other part and vice versa and therefore making it hard to generally raise the line. Therefore it is entirely within reason that if we completed the data set and took some measurements for low time of flight, then it would not look as promising any more. It might have been

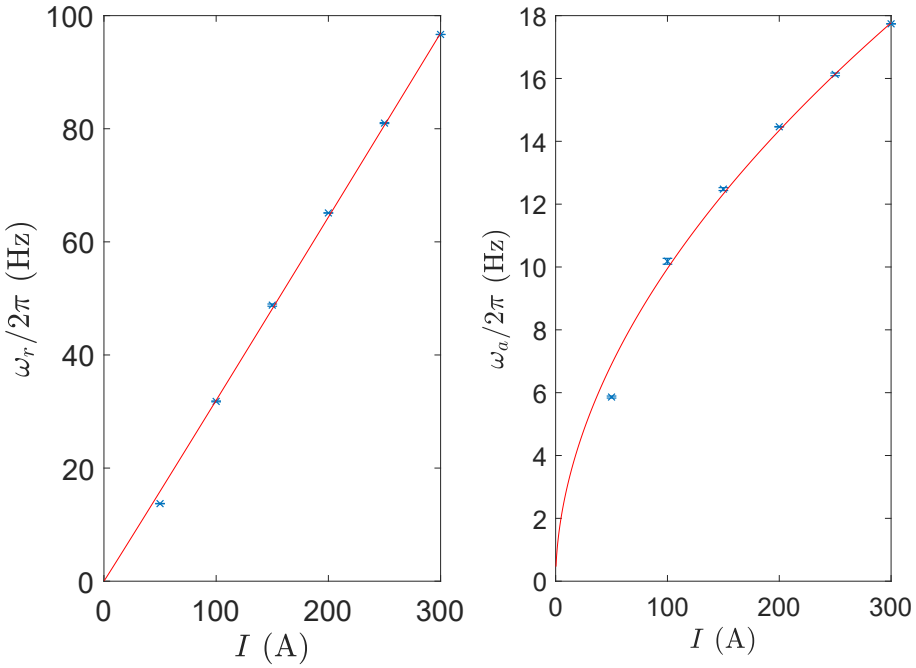

Figure 6.8: Experimental measurement of the "decay" of the trap frequencies at $I_{zShim} = 4$A, with $b_r = 1.0091 \pm 0.0709$ and $b_a = 0.5278 \pm 0.0642$.

enlightening to see what would happen and seeing how the individual widths would compare to the theoretical prediction, but unfortunately this is where we decided that we had spent enough time with these calibrations. Worth noting is also that Figure 6.9 was first produced after we finished the hunt for the β-calibration and we didn't have anything that looked quite as promising back then.

This still leaves some open questions. We still do not know why the simulations of the trap frequencies and the measurements are so different. We also don't really know the true extent of the influence from the eddy currents nor do we know the magnetic field the cloud feels during time of flight. Previously the shim coils were used to cancel the background field in all directions. However, this might have changed since the last calibration that was done years ago. Finding these null field currents would be the next logical step, but they were first done after I left active laboratory work.

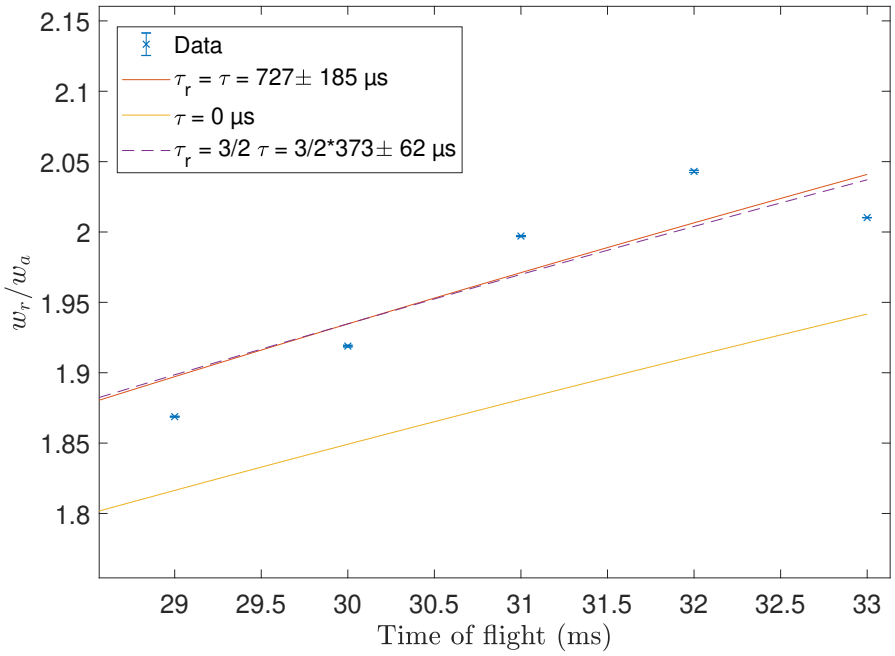

Figure 6.9: Aspect ratio for the decompressed trap with different trap decay parameters. For all lines $\tau_a = 0.5\tau$. Each data point include 3 runs.

Chapter 7

Conclusion and outlook

7.1 SkyFit

SkyFit is clearly working and able to give results that are closer to the theoretical predictions than its predecessor, increasing the accuracy of our measurements and making it a tool possible to use in the laboratories. With its extra features, SkyFit can hopefully allow us to get results requiring even higher precision in the future.

SkyFit can at its present state, do what is necessary in order to do evaluations, however as with most programs, there is always more things to be done. Doing the time of writing this, we are still working on the spatial α-calibrations and when these are done and well understood, SkyFit should be able to use these calibrations, as of the moment of writing, there is a framework that should make it easy to implement.

While this is written SkyFit is only able to do thermal atoms at $T \lesssim T_c$ (Bose-enhanced Gaussian) and at $T \gg T_c$ (pure Gaussian fit), but the in-between area the results might not yield the correct results. At some point the group might investigate the fugacity, and in that event this should also be implemented in SkyFit. Again, the framework is there, waiting for the results.

7.2 Spatial α calibration

The α calibration have been improved by our work, before the method used in [15] was fine with low photon numbers, but with our work, we can extend it to higher photon numbers, by using the absorbed amount per atom, instead of the total photon number. Making α depend on the atomic density, is also be a step in the right direction. Even if our work indicate there are still other effects that could influence

the imaging process, that are still unaccounted for.

Our work are able to improve our own accuracy when looking at absorption imaging and our methods are also applicable to other experiments, making it a successful investigation, even if we are not able to account for everything.

7.3 β calibration

The β calibration proved harder to make than we initially anticipated and the work is therefore left unfinished. We might have found a solution if we had continued the work, but it could have been time consuming, too much compared to the relative small gain, when other and more interesting experiments can be done, it is after all only a calibration and does not bring more physics with it. But we did learn that the axial and radial trap frequencies decay at different rates and that these rates are quite different. For this investigation we also developed a program able to simulate our magnetic trap, which is a tool that might come in handy at some later time.

Bibliography

[1]J. P. Dowling and G. J. Milburn, "Quantum technology: the second quantum revolution", Philosophical Transactions of the Royal Society of London. Series A: Mathematical, Physical and Engineering Sciences **361**, 1655–1674 (2003).

[2]S. Bose, "Planck's law and light quantum hypothesis", Z. Phys **26**, 178 (1924).

[3]A. Einstein, "Quantum theory of the monatomic ideal gas",

[4]A. Griffin, "A brief history of our understanding of bec: from bose to beliaev", arXiv preprint cond-mat/9901123 (1999).

[5]F. Dalfovo, S. Giorgini, L. P. Pitaevskii, and S. Stringari, "Theory of bose-einstein condensation in trapped gases", Rev. Mod. Phys. **71**, 463–512 (1999).

[6]M. H. Anderson, J. R. Ensher, M. R. Matthews, C. E. Wieman, and E. A. Cornell, "Observation of bose-einstein condensation in a dilute atomic vapor", science **269**, 198–201 (1995).

[7]K. B. Davis, M.-O. Mewes, M. R. Andrews, N. J. van Druten, D. S. Durfee, D. Kurn, and W. Ketterle, "Bose-einstein condensation in a gas of sodium atoms", Physical review letters **75**, 3969 (1995).

[8]C. C. Bradley, C. Sackett, J. Tollett, and R. G. Hulet, "Evidence of bose-einstein condensation in an atomic gas with attractive interactions", Physical review letters **75**, 1687 (1995).

[9]C. Pethick and H. Smith, *Bose-einsten condensation in dilute gases* (2008).

[10]W. Ketterle, D. S. Durfee, and D. Stamper-Kurn, "Making, probing and understanding bose-einstein condensates", arXiv preprint cond-mat/9904034 (1999).

[11]M. A. Kristensen, "Atom number fluctuations", PhD thesis (Department of Physics and Astronomy University of Aarhus, Denmark, 2018).

[12]Y. Castin and R. Dum, "Bose-einstein condensates in time dependent traps", Physical Review Letters **77**, 5315 (1996).

[13]P. Van der Straten and H. Metcalf, *Atoms and molecules interacting with light: atomic physics for the laser era* (Cambridge University Press, 2016).

[14]H. J. Metcalf and P. Van der Straten, "Laser cooling and trapping of neutral atoms", The Optics Encyclopedia: Basic Foundations and Practical Applications (2007).

[15]G. Reinaudi, T. Lahaye, Z. Wang, and D. Guéry-Odelin, "Strong saturation absorption imaging of dense clouds of ultracold atoms", Optics letters **32**, 3143–3145 (2007).

[16]P. L. Pedersen, "Multi-mode spin dynamics of a bose-einstein condensate in an optical lattice", PhD (Department of Physics and Astronomy University of Aarhus, Denmark, 2014).

[17]M. Gajdacz, "Non-destructive imaging and feedback with ultracold gases", PhD thesis (Department of Physics and Astronomy University of Aarhus, Denmark, 2015).

[18]W. H. Wing, "On neutral particle trapping in quasistatic electromagnetic fields", Progress in Quantum Electronics **8**, 181–199 (1984).

[19]D. J. Griffiths, *Introduction to electrodynamics*, 2005.

[20]H. J. Metcalf and P. van der Straten, "Laser cooling and trapping of neutral atoms", in *The optics encyclopedia* (American Cancer Society, 2007) Chap. 12.

[21]D. A. Steck, *Rubidium 87 d line data*, 2001.

[22]S. Dettmer, D. Hellweg, P. Ryytty, J. J. Arlt, W. Ertmer, K. Sengstock, D. Petrov, G. Shlyapnikov, H. Kreutzmann, L. Santos, et al., "Observation of phase fluctuations in elongated bose-einstein condensates", Physical Review Letters **87**, 160406 (2001).